

THE AGE, STELLAR CONTENT AND STAR FORMATION TIMESCALE OF THE B59 DENSE CORE

K. R. COVEY^{1,2,3,4}, C. J. LADA¹, C. ROMAN-ZUNIGA⁵, A. A. MUENCH¹, J. FORBRICH¹, J. ASCENSO¹

DRAFT July 19, 2010

ABSTRACT

We have investigated the stellar content of Barnard 59 (B59), the most active star-forming core in the Pipe Nebula. Using the SpeX spectrograph on the NASA Infrared Telescope Facility, we obtained moderate resolution, near-infrared (NIR) spectra for 20 candidate Young Stellar Objects (YSOs) in B59 and a representative sample of NIR and mid-IR bright sources distributed throughout the Pipe. Measuring luminosity and temperature sensitive features in these spectra, we identified likely background giant stars and measured each star's spectral type, extinction, and NIR continuum excess.

To measure B59's age, we place its candidate YSOs in the Hertzsprung-Russell (HR) diagram and compare their location to YSOs in several well studied star forming regions, as well as predictions of pre-main sequence evolutionary models. We find that B59 is composed of late type (K4-M6) low-mass ($0.9\text{--}0.1\text{ M}_{\odot}$) YSOs whose median stellar age is comparable to, if not slightly older than, that of YSOs within the ρ Oph, Taurus, and Chameleon star forming regions. Deriving absolute age estimates from pre-main sequence models computed by D'Antona et al., and accounting only for statistical uncertainties, we measure B59's median stellar age to be 2.6 ± 0.8 Myrs. Including potential systematic effects increases the error budget for B59's median (DM98) stellar age to $2.6^{+4.1}_{-2.6}$ Myrs. We also find that the relative age orderings implied by pre-main sequence evolutionary tracks depend on the range of stellar masses sampled, as model isochrones possess significantly different mass dependences.

The maximum likelihood median stellar age we measure for B59, and the region's observed gas properties, suggest that the B59 dense core has been stable against global collapse for roughly 6 dynamical timescales, and is actively forming stars with a star formation efficiency per dynamical time of $\sim 6\%$. While the $\sim 150\%$ uncertainties associated with our age measurement propagate directly into these derived star formation timescales, the maximum likelihood values nonetheless agree well with recent star formation simulations that incorporate various forms of support against collapse, such as sub-critical magnetic fields, outflows, and radiative feedback from protostellar heating.

Subject headings: Hertzsprung-Russell (HR) diagram – infrared: stars – stars: emission-line – stars: formation – stars: pre-main sequence

1. INTRODUCTION

The current consensus is that star formation progresses rapidly over a wide range of environments and spatial scales. This view is supported by observations that a stellar population's age spread is rarely larger than twice the system's crossing time ($\tau_{\text{cross}} = R_{\text{core}}/\sigma_v$ Elmegreen 2000) and that ongoing star formation appears ubiquitous within well known molecular clouds: there are few examples of clouds in a pre-star forming state, or of clouds associated with stellar populations older than ~ 5 Myrs (Hartmann et al. 2001; Ballesteros-Paredes & Hartmann 2007). Taken together, these observations suggest that star formation starts soon after a molecular cloud forms, and persists only a few dynamical times before the cloud is disrupted

or dissipates.

The Pipe Nebula (Alves et al. 2007) and California Molecular Cloud (Lada et al. 2009) are anomalies within this prompt star formation paradigm. Lacking major star formation activity, these molecular complexes have only recently begun to receive significant scrutiny. The first global study of the Pipe was the CO survey by Onishi et al. (1999), which identified 14 dense clumps that may be future sites of active star formation. Lombardi et al. (2006) then applied the NICER technique Lombardi & Alves (2001) to 2MASS data to construct an extinction map of the Pipe. This map, which is shown in Figure 1, leverages the dense screen of background stars provided by the Pipe's projection against the Galactic bulge, as well as its proximity ($d \sim 130$ pc; Lombardi et al. 2006), to resolve physical structures as small as 0.04 pc .

Studies of the Pipe's dense cores have begun to inform our understanding of the earliest stages of the star formation process. Using a wavelet filtering technique to identify individual dense cores in the Lombardi et al. extinction map, Alves et al. (2007) noted that the Pipe's dense core mass function qualitatively resembles the stellar mass functions measured in young clusters (e.g. Muench et al. 2002; Luhman 2004) and the field (Covey et al. 2008; Bastian et al. 2010), but with

¹ Harvard-Smithsonian Center for Astrophysics, 60 Garden Street, Cambridge, MA 02138

² Hubble Fellow

³ Current Address: Cornell University, Department of Astronomy, 226 Space Sciences Building, Ithaca, NY 14853

⁴ Visiting Astronomer at the Infrared Telescope Facility, which is operated by the University of Hawaii under Cooperative Agreement no. NCC 5-538 with the National Aeronautics and Space Administration, Science Mission Directorate, Planetary Astronomy Program.

⁵ Centro Astronómico Hispano Alemán/CSIC-IAA, Granada 18006, Spain

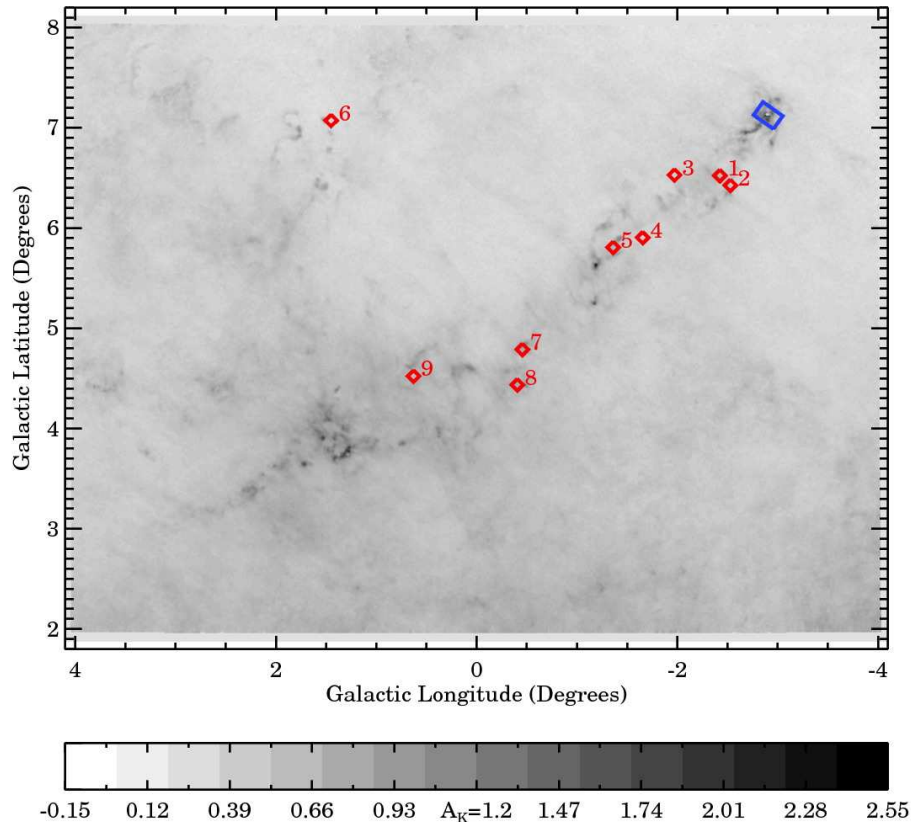


FIG. 1.— The locations of MIPS bright sources observed in this program (red diamonds), labelled with the [CLR2010] source number from Table 2. Provided for context is the NICER extinction map of the Pipe Nebula produced by Lombardi et al. (2006) (greyscale contours); the blue box in the upper right identifies the location of B59, shown in more detail in Figure 2.

a peak mass that is larger by a factor of three. Alves et al. interpreted this as evidence that the stellar mass function largely reflects the physics of core formation, with a global star formation efficiency of $\sim 33\%$ between the dense core and stellar stages. Subsequent studies have refined the mass function of Pipe cores, adopting physically motivated criteria to identify dense cores (Rathborne et al. 2009), and using detailed tests to verify the fidelity and completeness of the core mass function (Kainulainen et al. 2009). Other authors, however, have emphasized the difficulty of identifying coherent physical structures from two-dimensional column-density maps (e.g., Smith et al. 2008) and cautioned against making strict one-to-one comparisons between dense core and stellar mass functions (Swift & Williams 2008; Smith et al. 2009).

The physical properties of Pipe dense cores have also shed light on the formation and evolution of molecular clouds. A coordinated radio survey (Muench et al. 2007; Rathborne et al. 2008; Lada et al. 2008) identified thermal pressure as the dominant source of support against collapse for the Pipe’s dense cores, with non-thermal support limited to sub-sonic flows. With typical sizes of 0.1 parsec, and measured velocity dispersions of $0.1\text{--}0.2 \text{ km s}^{-1}$, these dense cores possess sound crossing times and minimum ages of ~ 1 million years. These core properties, and particularly their derived lifetimes, could help discriminate between

theoretical models where turbulence (Klessen et al. 2000; Mac Low & Klessen 2004; Offner et al. 2008) or magnetic fields (Nakano 1984; Shu et al. 1987; Mouschovias & Ciolek 1999; Nakamura & Li 2008) provide the dominant means of support for molecular cores. This evidence, however, is somewhat circumstantial, and relies on a critical assumption: that the Pipe’s dense core population will one day become active sites of ongoing star formation.

The Barnard 59 dense core (hereafter B59; originally dubbed the ‘Sinkhole’ by Barnard et al. 1927) could provide a clearer test for these theoretical models: as the only site of active star formation within the Pipe, no extrapolations of the core’s future behavior are necessary. While B59 is the Pipe’s most massive core, its physical properties (including the dominance of thermal motions) are nonetheless representative of the broader population of dense cores within the Pipe, making it an instructive case study. Since 1950, seven optically visible $H\alpha$ emitting stars (or unresolved multiple systems) have been associated with B59 (V359 Oph, KK Oph AB, LkH α 345 Oph, LkH α 346 Oph AB, KW 002, TH α 27-5, and LkH α 347 Oph; Merrill & Burwell 1950; The 1964; Stephenson & Sanduleak 1977; Kohoutek & Wehmeyer 2003; Herbig 2005). A recent Spitzer survey of B59 by Brooke et al. (2007) identified 16 additional candidate members with strong near-infrared (NIR) excesses, 4 of which were detected previously in the sub-mm

(Reipurth et al. 1996) or by IRAS at far infrared wavelengths. These sources appear to span a range of evolutionary states, from the low-mass, relatively embedded Class 0/I protostar studied by Riaz et al. (2009), to more revealed Class II sources. Analyses of Spitzer, ROSAT, and XMM observations of the Pipe Nebula confirm that B59 contains the vast majority of the Pipe’s recently formed stars (Forbrich et al. 2009, 2010).

The physical properties of the B59 dense core make it a good analog for modern computational simulations of the collapse of isolated dense cores. In this respect, characterizing the timescale and efficiency of star formation in the B59 dense core would provide a good opportunity to compare these empirically measured quantities with the predictions of these simulations. Various methods have been developed to estimate the ages of pre-main sequence stars, with differing advantages and levels of accuracy. The destruction of a star’s primordial lithium abundance has been used to estimate the ages of pre-main sequence stars with moderate success (i.e., typical uncertainties of ~ 10 Myrs for members of 10-30 Myr moving groups; Mentuch et al. 2008), but this method would be difficult to apply to B59’s YSOs: measuring lithium abundances requires high resolution, high S/N optical spectra that would be difficult to acquire for B59’s heavily extincted YSOs ($A_V \geq 5$ Brooke et al. 2007), and recent studies indicate that lithium depletion may not a good age indicator for young ($t < 10$ Myrs) T Tauri stars (Sestito et al. 2008). A pre-main sequence star’s surface gravity also rises as it contracts towards the main sequence, providing an additional opportunity to constrain the star’s age. Theoretical models suggest that a precision of 0.1 dex in $\log g$ can provide age estimates accurate to within 50% (see Figure 8, Doppmann et al. 2005), but this precision is difficult to achieve in practice. $\log g$ values have been measured for pre-main sequence stars with an accuracy of ~ 0.2 dex (Doppmann et al. 2005; Takagi et al. 2010, e.g.,), providing age estimates accurate to ~ 1 -2 Myrs, but as with lithium depletion studies, these measurements depend on precise measurements of line shapes and strengths, requiring observationally intensive high resolution, high signal-to-noise spectra: obtaining spectra of this quality for ~ 20 B59 YSOs would require multiple nights on an 8-meter class telescope. Surface gravity indicators have been developed for lower-resolution spectra, but these indicators typically depend on observations at J or shorter wavelengths, again difficult to obtain for B59 YSOs, and have a typical precision of ± 0.5 dex, providing somewhat poorer age discrimination than is available with standard HR diagram analyses (~ 3 -5 Myrs Gorlova et al. 2003; Allers et al. 2009).

To characterize the timescale, efficiency, and products of star formation within the Pipe Nebula, we have conducted the first spectroscopic census of B59’s stellar population. Our observations discriminate bona-fide B59 members from background giants in the Galactic bulge, and establish that these members are late type (K4-M6) low-mass (0.9 – $0.1 M_\odot$) young stellar objects (YSOs). We then derive estimates of the absolute and relative ages of B59’s YSOs by comparing their locations within the observational Hertzsprung–Russell diagram with theoretical models and YSOs in other well known clusters. We measure B59’s median stellar age to be $\sim 2.6^{+4.1}_{-2.6}$ Myrs; while the error bars on this measurement are significant,

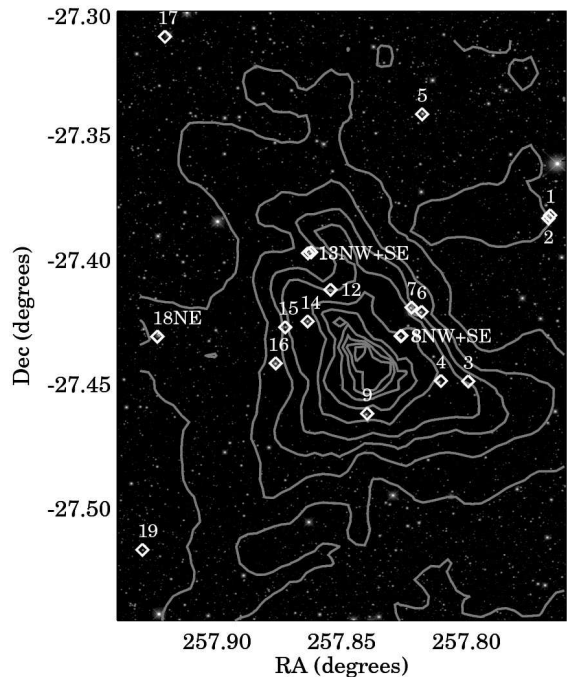


FIG. 2.— The K band image of B59 obtained by Román-Zúñiga et al. (2009), with locations of candidate YSOs observed in this program identified by diamonds and the source number assigned by Brooke et al. (2007). The NICER-based extinction map constructed by Román-Zúñiga et al. (2009) is shown for comparison as white contours. The lowest contour represents an extinction of $A_V = 2.5$; contours correspond to a 5 mag. increase in extinction up to $A_V = 22.5$, and increases of 10 mag. thereafter.

the maximum likelihood estimate implies that star formation has persisted within B59 for more than five times the current dynamical timescale and crossing time of B59’s dense gas.

In Section 2, we present our SpeX observations of candidate B59 members. Our method for measuring stellar parameters from these spectra is introduced in Section 3, along with our algorithm for placing those objects in the HR diagram and inferring ages and masses from pre-main sequence evolutionary models. We discuss our results in Section 4, and summarize our findings in Section 5. We also include a NIR spectral atlas of TW Hydrae members as an appendix to this work.

2. OBSERVATIONS

Using the SpeX spectrograph (Rayner et al. 2003) at NASA’s 2.5 meter Infrared Telescope Facility, we obtained low ($R \sim 200$) and moderate ($R \sim 2000$) resolution spectra of candidate young stellar objects (YSOs) in B59 and the Pipe Nebula. Observations were carried out during the early mornings of April 14-18 2008 (HST); typical seeing was $0.7''$, with clear skies interrupted by periods of light cirrus. The bulk of our observations were carried out in SpeX’s SXD mode with the $0.3''$ slit, providing nearly contiguous spectral coverage from 0.8 to 2.5 microns with a resolution of $R \sim 2000$. During a night of abnormally poor seeing ($\sim 1''$) we made use of the larger $0.5''$ slit, degrading the spectral resolution to $R \sim 1200$.

TABLE 1
IRTF/SPEX SXD OBSERVING LOG FOR CANDIDATE B59 MEMBERS

Source ID	RA	Dec	2MASS J	2MASS H	2MASS K_s	SXD itime	SXD slit	SXD J S/N	SXD H S/N	SXD K S/N	NTT H	NTT K
[BHB2007] 1	17:11:03.93	-27:22:55.08	10.46	8.99	7.76	240	0.3	152/52	243/49	293/114	9.29	8.29
[BHB2007] 2	17:11:04.12	-27:22:59.44	9.75	8.79	8.05	240	0.3	136/48	155/35	151/73	8.91	8.56
[BHB2007] 3	17:11:11.83	-27:26:54.98	14.09	12.62	11.76	6240	0.5/0.3	58/13	108/26	186/40	12.69	11.77
[BHB2007] 4	17:11:14.46	-27:26:54.45	11.62	10.42	9.63	1920	0.3	277/41	344/48	347/57	10.62	9.77
[BHB2007] 5	17:11:16.26	-27:20:28.82	11.23	9.70	9.07	1440	0.3	132/57	168/23	158/56	9.70	9.08
[BHB2007] 6	17:11:16.31	-27:25:14.50	10.58	9.37	8.75	960	0.3	203/40	234/41	227/63	9.37	8.75
[BHB2007] 7	17:11:17.28	-27:25:08.16	13.61	10.82	8.77	1920	0.3	58/12	261/34	325/92	10.58	8.77
[BHB2007] 8 NW	17:11:18.24	-27:25:48.94	1920	0.3	...	2/0	59/17	16.01	12.87
[BHB2007] 8 SE	17:11:18.32	-27:25:49.53	>18.4	15.12	11.95	1920	0.3	...	3/0	60/16	15.35	12.78
[BHB2007] 9	17:11:21.55	-27:27:41.70	12.74	10.57	8.98	2400	0.3	122/31	230/42	348/69	11.215	8.98
[BHB2007] 12	17:11:25.08	-27:24:42.67	16.52	13.61	11.57	2880	0.5	15/3	63/13	154/34	13.32	11.58
[BHB2007] 13 NW	17:11:26.95	-27:23:48.40	11.88	10.14	9.08	1440	0.3	84/32	126/42	120/3	10.14	9.08
[BHB2007] 14	17:11:27.28	-27:25:28.32	13.17	10.65	9.11	2400	0.5	120/21	351/31	494/111	10.57	11.44
[BHB2007] 15	17:11:29.43	-27:25:36.89	13.28	11.74	10.70	2400	0.5	149/24	291/30	359/46	11.74	10.58
[BHB2007] 16	17:11:30.35	-27:26:28.91	11.91	10.00	8.89	1680	0.3	49/19	64/32	64/66	10.23	9.19
[BHB2007] 17	17:11:41.00	-27:18:36.82	10.64	8.75	7.54	960	0.3	146/18	150/8	106/19	8.75	7.54
[BHB2007] 18 NE	17:11:41.73	-27:25:50.26	480	0.3	216/37	287/39	312/50	10.46	9.86
[BHB2007] 18 SW	1440	0.3	72/32	76/40	69/55
[BHB2007] 19	17:11:43.17	-27:30:58.54	14.09	12.75	11.91	1920	0.3	47/11	92/17	127/26	12.66	11.74
[BHB2007] 20	17:12:00.20	-27:20:18.10	10.54	9.64	9.17	960	0.3	119/51	116/51	146/81	9.641	9.17
V359 Oph	17:08:54.28	-27:12:33.03	9.73	9.12	8.80
LkH α 345	17:10:48.04	-27:40:51.19	9.60	8.69	8.35
KK Oph A	17:10:08.07	-27:15:18.24	9.07	7.23	5.80

For maximum observational efficiency, we chose not use the image rotator to align the slit with the parallactic angle over the course of each night. Spectra of telluric standards taken at slit rotations that differ by 30-60° suggest that color-dependent slit losses due to atmospheric refraction are relatively minor, altering the slope of the spectral energy distribution (SED) between the J and K bands by less than 10%. During our last night of observations we also utilized SpeX's high-throughput, low-resolution ($R \sim 200$) prism mode to obtain high fidelity NIR SEDs for candidate YSOs in B59. During these observations, care was taken to align the slit to within 10° of the parallactic angle, except in cases where the slit was rotated to allow observations of individual components of an apparent multiple system.

Brooke et al. (2007) identified candidate YSOs in B59 by searching for IR excesses in spectral energy distributions (SEDs) constructed from 2MASS, IRAC and MIPS photometry. For the remainder of this paper, we identify these candidate YSOs with a [BHB2007] prefix, followed by the source ID assigned by Brooke et al. in their Table 1. We obtained spectra for each of these candidate B59 members, with the exception of two objects too faint to observe with SpeX ([BHB2007] 10, & 11). A K band image of B59 observed by Román-Zúñiga et al. (2009) is shown in Figure 2, overplotted with the locations of the candidate YSOs observed in this program. Our SXD observations are summarized in Table 1, where we indicate the slit width and exposure time used to obtain each source's spectrum. We include for completeness the 2MASS position and magnitudes for each source as well as H and K band magnitudes measured by Román-Zúñiga et al. (2009) from their NTT images of the cluster. We also include positions and 2MASS magnitudes for 3 likely B59 members (V359 Oph, KK Oph AB, and LkH α 345 Oph) with spectral types in the literature that suffice to place each star in the HR diagram.

To characterize the more extended population of bright

IR objects that extends across the Pipe, we obtained spectra for a sample of objects with $K < 10$ (to ensure accessibility to SpeX) and detections at both 24 and 70 microns in an extensive Spitzer survey of the Pipe Nebula (Forbrich et al. 2009). The locations of these sources are indicated in Figure 1, and their NIR properties are listed in the top tier of Table 2. We observed all four sources ([CLR2010]⁶ 1, 2, 5 and 7) that met our flux criteria and are located within high extinction peaks identified by Alves et al. (2007), as we considered these sources the most likely bona fide YSO candidates. We additionally observed 6 similar sources that are not associated with extinction cores ([CLR2010] 3, 4, 6, 8 and 9). According to the criteria of Forbrich et al. (2009), two of the sources in our sample ([CLR2010] 1 & 2) are MIPS excess sources. A third source, [CLR2010] 7, has a MIPS spectral index marginally qualifying as class II but is not listed by Forbrich et al. (2009) due to a position mismatch at the source detection stage.

The SpeX spectral atlas⁷ (Cushing et al. 2005, Rayner et al., in prep; Vacca et al., in prep.) samples many spectral types and luminosity classes. To supplement this grid of standards with stars possessing pre-main sequence surface gravities, we observed members of the TW Hydrae moving group and ρ Ophiuchus cluster. The pre-main sequence standards are listed in the bottom tier of Table 2, and spectra of the TW Hya members are shown in Appendix A.

All data were reduced using SpeX's dedicated IDL reduction package, SpeXtool (Cushing et al. 2004). Telluric absorption was removed using observations of A0V stars at airmasses similar to those of the target

⁶ For consistency with the [BHB2007] designation adopted for the candidate B59 members identified by Brooke et al. (2007), we adopt a source designation of [CLR2010], followed by the source number given in Table 2, for the IR bright sources we observed throughout the Pipe.

⁷ available online at
[http://irtfweb.ifa.hawaii.edu/\\$\sim\\$spex/spexlibrary/IRTFlibrary.html](http://irtfweb.ifa.hawaii.edu/\simspex/spexlibrary/IRTFlibrary.html)

TABLE 2
IRTF/SPEX SXD OBSERVING LOG FOR PIPE/TW HYA SOURCES

Source ID	RA	Dec	2MASS J	2MASS H	2MASS K_s	SXD itime	SXD slit	SXD J S/N	SXD H S/N	SXD K S/N
[CLR2010] 1	17:14:51.08	-27:22:39.96	10.26	8.89	8.16	360	0.3	447/55	654/54	498/84
[CLR2010] 2 NE	480	0.3	100/44	107/33	106/36
[CLR2010] 2 SW	17:14:56.49	-27:31:08.08	10.42	9.56	9.04	480	0.3	86/32	100/32	108/35
[CLR2010] 3	17:15:59.37	-27:00:24.75	6.99	5.72	5.13	120	0.3	507/116	794/19	935/58
[CLR2010] 4	17:19:06.05	-27:06:18.95	13.07	9.69	7.50	360	0.3	25/5	136/9	141/38
[CLR2010] 5	17:20:12.47	-26:55:09.40	9.12	7.58	6.67	720	0.3	229/30	241/10	294/24
[CLR2010] 6	17:22:31.01	-23:53:48.76	7.52	6.06	5.13	120	0.3	357/17	474/9	884/21
[CLR2010] 7	17:26:15.14	-26:44:37.31	9.16	7.13	5.79	240	0.3	180/64	180/20	182/62
[CLR2010] 8	17:27:41.56	-26:53:46.7	10.12	7.87	6.19	240	0.3	38/15	146/43	488/49
[CLR2010] 9	17:29:54.08	-25:59:12.79	7.29	5.83	5.05	120	0.3	423/78	726/18	971/56
TW Hya 12	11:21:05.6	-38:45:16	9.00	8.33	8.05	480	0.3	343/113	392/46	346/88
CD 29-8887 A	11:09:14.0	-30:01:39	7.85	...	7.18	360	0.3	628/110	776/50	717/100
CD 29-8887 B	11:09:14.2	-30:01:38	9.09	...	7.99	480	0.3	434/107	451/51	352/103
CD 33-7795 A	11:31:55.4	-34:36:27	7.67	6.99	6.74	360	0.3	574/105	674/55	608/93
CD 34-7390 A	11:21:17.3	-34:46:47	8.43	7.73	7.49	120	0.3	241/96	290/48	267/91
CD 34-7390 B	11:21:17.5	-34:46:44	240	0.3	376/116	473/46	430/87
CD 36-7429 A	11:48:24.2	-37:28:49	8.60	7.95	7.68	480	0.3	392/99	420/47	343/87
CD 36-7429 B	11:48:24.0	-37:28:49	10.06	9.41	9.14	480	0.3	219/115	265/51	238/86
GSC 6659-1080 A	11:32:41.3	-26:51:55	8.34	7.66	7.43	120	0.3	239/104	285/48	262/81
GSC 6659-1080 B	11:32:41.2	-26:52:08	9.84	9.28	9.01	240	0.3	181/77	202/44	201/49
GSC 7766-074	12:35:04.4	-41:36:39	9.12	8.48	8.19	360	0.3	227/99	258/51	224/87
GY 17	16:26:23.7	-24:43:13.9	9.39	8.40	7.85	480	0.3	371/71	435/57	377/93
GY 250	16:27:19.5	-24:41:40.5	9.42	8.63	8.41	480	0.3	540/93	619/48	514/91
GY 292	16:27:33.1	-24:41:15.7	11.32	9.13	7.81	480	0.3	136/29	151/41	114/85
GY 93	16:26:41.26	-24:40:18	10.77	9.77	9.27	480	0.3	303/55	330/39	281/42
HD 98800 A	11:22:05.5	-24:46:39.7	6.40	5.76	5.59	360	0.3	863/84	970/46	783/77
Hen 3600 A	11:10:28.0	-37:31:53	8.22	7.60	7.28	360	0.3	269/117	325/49	315/68
Hen 3600 B	11:10:28.05	-37:31:54.2	8.63	8.07	7.80	360	0.3	213/95	245/49	223/75
SSS 1207-324	12:07:27.4	-32:47:00	8.62	8.02	7.75	360	0.3	319/112	364/53	329/78
TW Hya	11:01:52.0	-34:42:17	8.22	7.56	7.30	480	0.3	501/110	640/57	615/117
TYC 7760-0283	12:15:30.8	-39:48:42	8.17	7.50	7.31	360	0.3	434/111	525/46	461/82

($\Delta\text{sech} \lesssim 0.1$). Hydrogen features were removed from the A0V spectra by dividing by a model of Vega, and the target's true spectral slope and absolute flux densities were recovered by multiplying the target spectrum by a $\sim 10,000$ K blackbody spectrum scaled to match that of the telluric standard (Vacca et al. 2003). Tables 1 and 2 list the signal-to-noise (S/N) levels measured in the J, H and K_s bands of each source's reduced SXD spectrum. Two S/N estimates are listed for each band: the first estimate is the S/N calculated directly by SpeXtool. The second estimate is an empirical lower limit to each spectrum's S/N generated from the standard deviation of relatively featureless regions in each band (J: 1.215-1.235 μm , H: 1.52-1.54 μm , K: 2.13-2.15 μm).

3. ANALYSIS

We have analyzed these SpeX spectra to distinguish bona fide B59 members from contaminating background giants, and to infer the physical properties of each YSO. In §3.1, 3.2 and 3.3, we describe an iterative technique that identifies the spectral type, extinction and veiling that best reproduce the individual features and overall shape of each candidate B59 YSO's spectrum. In §3.4, we supplement these spectral measurements with photometry from the literature to estimate the effective temperature (T_{eff}) and bolometric luminosity (L_{bol}) of each target. Placing these YSOs in an observational Hertzsprung-Russell (H-R) diagram, we used pre-main sequence evolutionary models to infer masses and ages for each object. We present in §3.5 an estimate of B59's absolute age, as well as a relative age estimate derived from comparison to other clusters with similarly homo-

geneous photometric and spectroscopic datasets.

3.1. Estimating Extinction & Veiling From Synthetic Photometry

Following Meyer et al. (1997), we assume that a YSO's observed NIR color (e.g., $(J - H)_{\text{obs}}$) is due solely to its intrinsic photospheric color (e.g., $(J - H)_{\text{int}}$), an additional continuum excess from their circumstellar disk (e.g., $\Delta(J - H)$), such that $(J - H)_{\text{CTTS}} = (J - H)_{\text{int}} + \Delta(J - H)$, and an independent extinction/reddening term (e.g., $E(J - H) = 0.613 \times A_H$; $(J - H)_{\text{obs}} = (J - H)_{\text{CTTS}} + E(J - H)$). Algebraically combining the Meyer et al. (1997) CTTS locus (transformed onto the 2MASS photometric system) with a well behaved extinction law⁸ then requires a unique combination of reddening and disk excesses/veiling to reconcile a YSO's intrinsic and observed $(J - H)$ and $(H - K_s)$ colors:

$$A_H = 2.512 \times (J - H)_{\text{obs}} - 1.527 \times (H - K_s)_{\text{obs}} - 1.254 \quad (1)$$

$$\Delta(J - H) = (J - H)_{\text{obs}} - 0.613 \times A_H - (J - H)_{\text{int}} \quad (2)$$

⁸ Román-Zúñiga et al. (2007) measured the near/mid-IR extinction law in B59 itself, identifying A_J/A_K and A_H/A_K ratios that agree within 1σ of the values measured by Indebetouw et al. (2005) from large numbers of 2MASS stars. Given the agreement between these two studies, we adopt the Indebetouw et al. (2005) extinction law for maximum compatibility with the 2MASS photometry we utilize to characterize YSOs in B59 and other star formation regions.

TABLE 3
SPECTRAL LINE INDICES

Line Name	Line Center (μ)	Line Width (μ)	Cont. 1 Center (μ)	Cont. 1 Width (μ)	Cont. 2 Center (μ)	Cont. 2 Width (μ)
Mg 1.50	1.504	0.004	1.498	0.0045	1.5095	0.0045
K 1.52	1.5172	0.004	1.5105	0.004	1.523	0.004
Mg 1.58	1.576	0.004	1.57	0.004	1.58	0.004
Si 1.59	1.59	0.005	1.586	0.003	1.594	0.003
CO 1.62	1.61975	0.0045	1.615	0.003	1.628	0.003
CO 1.66	1.6625	0.004	1.6565	0.003	1.67	0.003
Al 1.67	1.674	0.006	1.659	0.003	1.678	0.002
1.70 dip	1.7075	0.003	1.704	0.003	1.7145	0.003
Mg 1.71	1.7115	0.003	1.704	0.003	1.7145	0.003
Ca 1.98	1.982	0.013	1.9676	0.005	1.99775	0.005
Na 2.21	2.2075	0.007	2.195	0.004	2.217	0.006
Ca 2.26	2.264	0.007	2.258	0.0045	2.27	0.0045
CO 2.3	2.30375	0.0225	2.288	0.007	2.3185	0.004
CO 2.34	2.3455	0.003	2.3425	0.003	2.349	0.003

$$\Delta(H - K_s) = (H - K_s)_{obs} - 0.354 \times A_H - (H - K_s)_{int} \quad (3)$$

YSOs often demonstrate considerable photometric variability, including in the NIR regime we focus on here (e.g., Carpenter 2001; Morales-Calderón et al. 2009). To estimate each YSO’s extinction and NIR excess at the exact epoch that the spectra were obtained, we calculate synthetic NIR photometry from each target’s SpeX spectrum following the prescription presented by Covey et al. (2007) in their §3.3.1. Using these JHK magnitudes, and assuming intrinsic photospheric colors characteristic of K7/M0 type stars, we can therefore obtain a good initial estimate of each YSO’s extinction (A_H) and $\Delta(J-H)$ and $\Delta(H-K_s)$ color excesses.

3.2. Extinction and Veiling Resistant Spectral Classification

Numerous investigators have identified H and K band spectral indices sensitive to a star’s luminosity class and spectral type (Kleinmann & Hall 1986; Ali et al. 1995; Wallace & Hinkle 1997; Meyer et al. 1998; Aspin 2003; Ivanov et al. 2004; Allers et al. 2007). We present in Table 3 a set of indices well suited for measuring stellar spectral types from moderate resolution ($R \sim 1000$ – 2000) spectra. Each feature’s local continuum is measured from a linear fit to the median flux in two nearby regions (‘Cont. 1’ and ‘Cont. 2’ in Table 3). Integrating the difference between the expected continuum and the actual flux in the line (defined by the ‘Line Center’ and ‘Line Width’ columns of Table 3), and dividing by the continuum flux density in the center of the line region, provides an Equivalent Width (EqW) measure of the strength of each feature. Equivalent width measures are convenient for spectral classification of YSOs: equivalent widths are relatively insensitive to extinction, which affects both the line and the local continuum equally, and ratios of closely separated lines are relatively robust to excess continuum flux, as both lines will be diluted equally and the sum effect will cancel out.

The strength and shape of water absorption in the H and K bands has also been identified by numerous authors as a useful spectral type and luminosity class indicator (e.g., Wilking et al. 1999; Reid et al. 2001;

Geballe et al. 2002; McLean et al. 2003; Slesnick et al. 2004; Allers et al. 2007; Weights et al. 2009), but is less amenable to characterization as an Equivalent Width. We defined two indices to characterize water absorption in the H and K bands; these indices are calculated as:

$$\text{Index} = \frac{\langle \text{Band1} \rangle / \langle \text{Band2} \rangle}{\langle \text{Band2} \rangle / \langle \text{Band3} \rangle} \quad (4)$$

where $\langle X \rangle$ simply denotes the mean flux level within the range of each band as given in Table 4.

To account for any residual sensitivity to extinction or veiling in our spectral indices, we compared our target’s index values to those measured from artificially reddened and veiled spectral standards. As described in §3.1, synthetic photometry from each SpeX spectrum produces an initial estimate of each target’s extinction and $(J-H)/(H-K)$ color excesses assuming the standard K7/M0 spectral type. Adopting the characteristic J band veiling ($r_J = \frac{F_{ex}}{F_*} = 0.25$) measured by Cieza et al. (2005) for a large sample of CTTSs sets the initial absolute scale for the veiling fluxes implied by each source’s $\Delta(J-H)$ and $\Delta(H-K_s)$ color excesses:

$$\begin{aligned} \Delta J &= 2.5 \times \text{Log}(r_J + 1) \\ \Delta H &= \Delta J + \Delta(J - H) \\ r_H &= 10^{\frac{\Delta H}{2.5}} - 1 \end{aligned} \quad (5)$$

We then iteratively adjusted each target’s assumed absolute J band veiling and spectral type (and thus intrinsic photospheric colors) to identify the self-consistent spectral type/extinction/veiling combination that best replicated the target’s measured spectral indices and overall SED shape. Figures 3 and 4 demonstrate our two dimensional spectral classification of GY 292 and [BHB2007] 5, respectively. GY 292 appears to be moderately veiled ($\Delta(J-H)$: 0.22; $\Delta(H-K_s)$: 0.35), but [BHB2007] 5 shows no evidence for veiling, so these two stars demonstrate the sensitivity of these spectral indices to the presence of veiling. Veiling has the largest impact on the two water indices shown in the upper left panels of Figures 3 and 4: standards veiled to match GY 292 are significantly compressed compared to the unveiled standards used to type [BHB2007] 5.

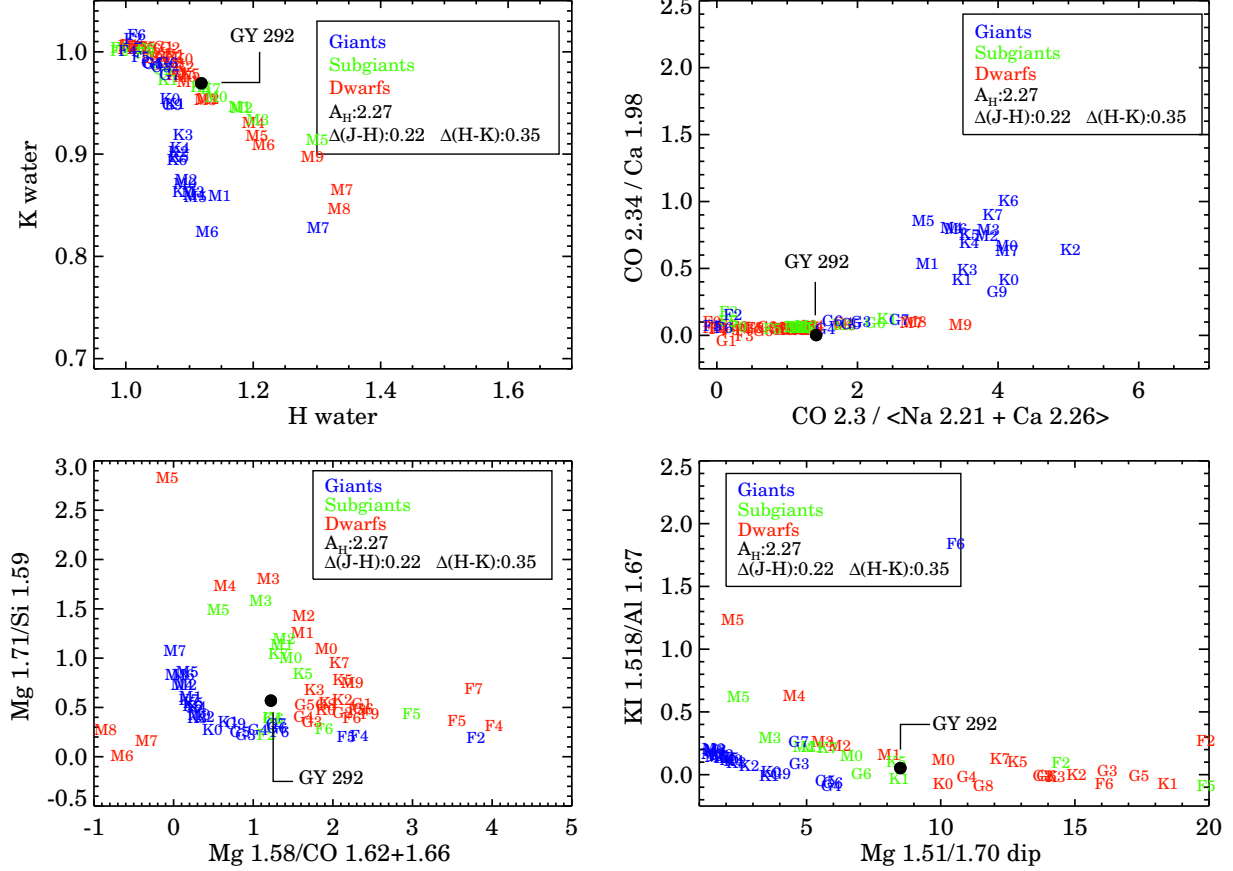


FIG. 3.— Two dimensional spectral classification of GY 292: each panel shows luminosity and gravity sensitive H and K band spectral indices presented in §3.2. Indices measured from GY 292, a confirmed YSO with a previously measured K8 spectral type (Luhman & Rieke 1999), are shown as a filled black point, while indices measured from spectral standards are labeled according spectral type, and color-coded according to luminosity class. Standard spectra were artificially veiled and extinguished to match estimates from GY 292’s photometry and spectra before indices were measured. GY 292 appears to be an \sim K5 object with subgiant-like surface gravity, as expected for a bona-fide YSO.

TABLE 4
WATER INDICES

Name	Band 1	Band 2	Band 3
H ₂ O-H	1.595-1.615	1.68-1.70	1.76-1.78
H ₂ O-K	2.18-2.20	2.27-2.29	2.36-2.38

Figure 4 also demonstrates the utility of two-dimensional spectral classification for identifying background giants, as [BHB2007] 5 is clearly identified in each plot as a giant star; lacking significant veiling, or emission lines indicative of mass accretion, this object appears to be a background late K/early M giant star.

3.3. Derived Spectral Types

Applying our classification algorithm to these spectra identifies two of the B59 candidate YSOs and the majority of the IR excess stars throughout the Pipe as likely giants: we classify [BHB2007] 5, [CLR2010] 3 and 9 as reddened giants or supergiants, [CLR2010] 8 as a giant carbon star, and [CLR2010] 4, 5, 6 and [BHB2007] 17 as OH/IR stars, likely residing in the Galactic Bulge. The spectra of these stars are shown in Figure 5 along with

spectra of known giants obtained by Lançon & Wood (2000) and Cushing et al. (2005). Our classification of [BHB2007] 5 and 17 as background giants is reinforced by their non-detection at X-ray wavelengths in an XMM pointing containing B59 (Forbrich et al. 2010, in press).

The spectra of the confirmed B59 YSOs are shown in Figures 6 and 7, with their derived spectral types, extinctions, and JHK veilings presented in Table 5. We tested the accuracy of these results by comparing the parameters we measure for four ρ Oph YSOs to those reported by Luhman & Rieke (1999). We derived spectral types for GY 292 (K5), GY 17 (K5), GY 250 (M1) and GY 93 (M5); Luhman & Rieke (1999) derived spectral types for these objects of K8, K6, M0, and M4 respectively. The types assigned to GY 17, 93, and 250 agree within 1 subclass, while the type we assign to GY 292 is earlier by two/three subclasses (following Kirkpatrick et al. 1991, our classification scheme omits types K6 and K8). On the basis of this comparison, we adopt a conservative uncertainty of ± 2 subclasses in our derived spectral types. Similarly, comparing the extinctions and veilings we derive with those reported by Luhman & Rieke (1999) suggest that we achieve $\sigma_{A_H} \approx 0.5$ mag and $\sigma_{\tau_K} \approx 0.35$.

Two sources, [CLR2010] 1 and 7, present somewhat

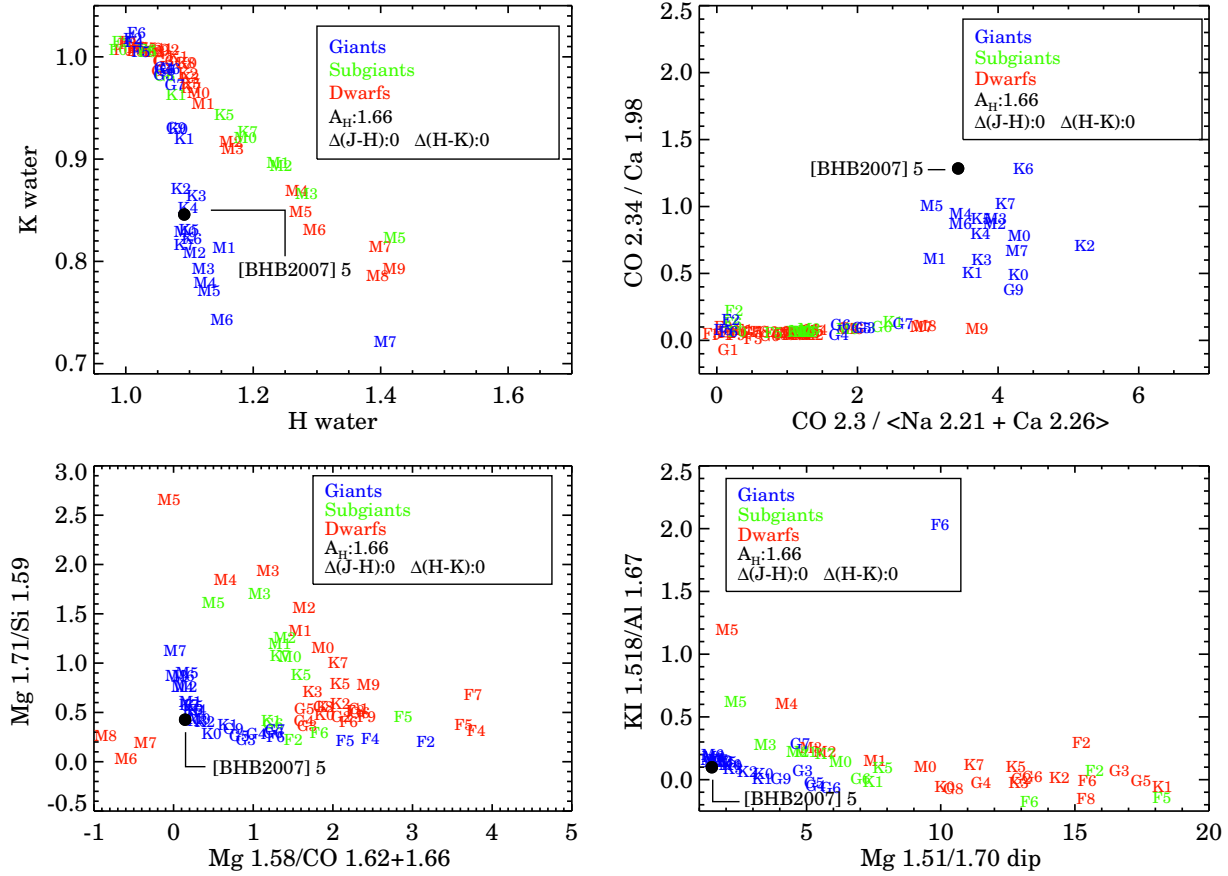


FIG. 4.— The two dimensional spectral classification plots for candidate YSO [BHB2007] 5; symbols are as in Figure 3. [BHB2007] 5 appears to be a mid-late K star, with giant-like surface gravity; visual inspection of its spectrum confirms it as a background giant rather than a bona-fide YSO (see Fig. 5).

ambiguous spectra. [CLR2010] 7 possesses a sub-giant/giant-like surface gravity, with prominent Paschen β , Paschen γ , and Brackett γ emission features as seen in some YSOs. [CLR2010] 7 is also located on the edge of a Pipe extinction core, and is on the lower boundary defined by Forbrich et al. (2009) to select candidate class II sources based on their MIPS spectral index. While these properties are consistent with a YSO classification, Ojha et al. (2007) identify [CLR2010] 7 as a likely high mass-loss AGB star in the Galactic Bulge in their analysis of detections by the Mid-course Space Experiment. This classification is also consistent with the observed properties of [CLR2010] 7, explaining its strong HI emission as a signature of strong stellar winds. We tentatively classify this source as a giant star, and include its spectrum in Figure 5. [CLR2010] 1 is more ambiguous: this source possesses a low (sub-giant) surface gravity, and has a location in the HR diagram consistent with that of other B59 members (see §3.3 for a discussion of HR diagram placement). This HR diagram location implies a rather young age for [CLR2010] 1, however, which is somewhat inconsistent with the source's lack of NIR excess/disk emission or mass accretion sensitive emission lines. Indeed, [CLR2010] 1's NIR photometry is also consistent with that of a reddened background giant/sub-giant. Definitively resolving [CLR2010] 1's status will require additional observations; for now we include it in

Table 5 and Fig. 6 as a potential Pipe YSO, but exclude it from our population analysis of B59 members.

One of the IR excess stars located outside of B59, however, is likely a newly identified YSO. [CLR2010] 2 lies in the stem of the Pipe, within an Alves et al. (2007) extinction core (see Fig. 1 for its exact location), and was identified by Forbrich et al. (2009) as a new candidate YSO (source 16 in their object list). While detected as a single source by MIPS, [CLR2010] 2 proved to be a visual binary when observed with SpeX: we obtained spectra of both the NE and SW components, and the spectral indices measured from both sources are consistent with pre-main sequence surface gravities. Strong HI, HeI, and Ca II emission lines are also visible in the spectrum of [CLR2010] 2 SW, consistent with the source being an actively accreting YSO. This source was also identified as an H α emission line source by Kohoutek & Wehmeyer (2003), indicating that the HI emission persists over long timescales. These observations suggest that [CLR2010] 2 SW is a bona fide YSO associated with the Pipe Nebula, and [CLR2010] 2 NE is a promising candidate as well. The detection of H α from [CLR2010] 2, and the low extinction estimates we derive from our SpeX observations, indicate that follow-up optical spectroscopy of the 6707 Å Li line may be a tractable means of definitively resolving each component's pre-main sequence status. As with [CLR2010] 1, we include [CLR2010] 2 NE and SW in

TABLE 5
MEASURED SPECTRAL PARAMETERS

Source	SpT ^a	A_H	r_J	$\Delta J-H$	r_H	$\Delta H-K$	r_K	Br γ ?	low log g ?	YSO
[BHB2007] 1	K7	0.84	0.26	0.05	0.32	0.30	0.76	Y	Y	Y
[BHB2007] 2	M3	0.68	0.00	0.00	0.00	0.00	0.00	W	Y	Y
[BHB2007] 3	M6	1.43	0.00	0.00	0.00	0.00	0.00	?	N	?
[BHB2007] 4	M5	0.74	0.26	0.10	0.39	0.16	0.62	Y	Y	Y
[BHB2007] 6	M2	0.97	0.00	0.00	0.00	0.00	0.00	N	Y	Y
[BHB2007] 7	K5:	2.80	0.45	0.44	1.16	0.69	3.11	Y	Y	Y
[BHB2007] 8NW ^b	K/M:	2.41	1.20	1.54	11.5	N	?	?
[BHB2007] 8SE ^b	M:	4.54	0.26	3.89	1.34	N	?	?
[BHB2007] 9	K5	1.34	0.38	0.39	0.97	0.61	2.48	Y	Y	Y
[BHB2007] 12	M5	3.00	0.26	0.13	0.42	0.27	0.73	Y	Y	Y
[BHB2007] 13NW	M2	2.18	0.15	0.00	0.15	0.00	0.15	W?	Y	Y
[BHB2007] 14	K5	2.48	0.38	0.38	0.96	0.60	2.43	Y	Y	Y
[BHB2007] 15	M6	1.74	0.00	0.01	0.01	0.01	0.03	N	Y	Y
[BHB2007] 16	K4:	1.83	0.32	0.09	0.44	0.12	0.61	N	Y	Y
[BHB2007] 18NE	M5	0.60	0.26	0.15	0.45	0.25	0.83	Y	Y	Y
[BHB2007] 18SW	M2:	0.76	0.26	0.12	0.41	0.27	0.83	W	Y	Y
[BHB2007] 19	M3:	1.36	0.25	0.0	0.25	0.00	0.25	Y	Y?	Y
[BHB2007] 20	M2	0.48	0.38	0.04	0.43	0.13	0.63	Y	Y	Y
[CLR2010] 2NE	M3	0.20	0.25	0.00	0.25	0.18	0.48	W?	Y?	Y?
[CLR2010] 2SW	M5	0.20	0.25	0.12	0.40	0.19	0.67	Y	Y?	Y?
[CLR2010] 1	M1	1.30	0.25	0.00	0.25	0.00	0.25	N	Y	?

^a Spectral types flagged with colons are derived from somewhat noisy spectra, resulting in less certain derived spectral types.

^b Spectra are extremely noisy, and lack data in the J band; measurements of r_J and $\Delta(J-H)$ are impossible, and other measurements are very low quality.

Table 5 and Figs. 6 and 7.

3.4. Calculating T_{eff} and L_{bol}

To compare the properties of B59's YSOs with theoretical models of pre-main sequence evolution, we adopted the SpT to T_{eff} conversion developed by Luhman et al. (1998). The T_{eff} implied by each source's spectral type is shown in Table 6. In the spectral type range occupied by most B59 members, our ± 2 subclass spectral type uncertainty corresponds to an ~ 300 K uncertainty in temperature.

With extinction and veiling estimates for each candidate B59 member, we are able to calculate stellar luminosities from their NIR photometry. We followed Hillenbrand (1997) in calculating each YSO's bolometric luminosity as:

$$\text{Log}(L_{tot}/L_{\odot}) = 0.4 \times \left(4.75 - (H - A_H - DM + BC_H) \right) \quad (6)$$

where DM is the distance modulus to B59 ($d=130$ pc, $DM = 5.569$; Lombardi et al. 2006) and BC_H is the H band bolometric correction for each star's spectral type as tabulated by Kenyon & Hartmann (1995); the values adopted for each star are included for reference in Table 6.

We also calculate the purely stellar component of each YSOs bolometric luminosity by removing the H band veiling flux, expressed in magnitudes (see §3.2 for the transformation between the veiling flux ratio in a given band (e.g., r_H) and the photometric excess in that band (e.g., ΔH):

$$\text{Log}(L_{stel}/L_{\odot}) = 0.4 \times$$

$$\left(4.75 - (H + \Delta H - A_H - DM + BC_H) \right) \quad (7)$$

We adopt the measured 2MASS H band magnitude for isolated B59 members in this calculation, enabling us to perform an identical analysis of YSOs with known spectral types in other well studied star forming regions. Objects with nearby ($<4''$) companions may be blended in 2MASS due to that survey's relatively large pixels ($\sim 2''$); for those sources ([BHB2007] 2, 8 NW & SE, 13 NW, 18 NE & SW; [CLR2010] 2 NE & SW), we adopt the synthetic H band magnitude measured from our spectra, noting that the SpeXTool reduction pipeline produces spectra with a first-order correction for slit losses derived from the observations of the telluric standard.

Both luminosity estimates (total and stellar-only) are listed in Table 6 and shown in Figure 8. Accounting for the uncertainties in each of the input parameters results in a total uncertainty for these luminosity estimates of 0.3 dex. The difference between the total and stellar luminosity estimated for a given YSO is usually less than 0.2 dex, indicating that the veiling correction, while not negligible, does not exceed the overall error in each YSO's location in the HR diagram.

3.5. Inferring B59's Median Stellar Age

We have used the pre-main sequence (PMS) evolutionary models calculated by D'Antona & Mazzitelli (1994) and updated in 1998 (DM98 hereafter), and those calculated by Baraffe et al. (1998), to infer the age and mass of each candidate B59 YSO. These parameters were determined by interpolating between model points with temperatures and luminosities similar to that of each YSO. These theoretical models do not account for accretion luminosity, so for this comparison we adopted the veiling subtracted value of L_{stel} for each YSO. Table 6 presents masses and ages derived for candidate B59 members with

TABLE 6
INFERRED STELLAR PARAMETERS

Source	T_{eff}	BC_H	$\text{Log } \frac{L_{tot}}{L_{\odot}}$	$\text{Log } \frac{L_{stel}}{L_{\odot}}$	DM98 Age (Myr)	DM98 Mass (M_{\odot})	B98 Age (Myr)	B98 Mass (M_{\odot})
[BHB2007] 1	4060.	2.11	0.02	-0.10	0.79	0.49	4.37	1.14
[BHB2007] 2	3346.	2.37	-0.03	-0.03	≤ 0.07	0.20	≤ 1.0	0.60
[BHB2007] 3	2841.	2.58	-1.38	-1.38	2.59	0.09	≤ 1.0	0.07
[BHB2007] 4	3009.	2.51	-0.75	-0.89	1.04	0.14	≤ 1.0	0.14
[BHB2007] 6	3514.	2.27	-0.14	-0.14	0.15	0.24	≤ 1.0	0.62
[BHB2007] 7	4350.	2.02	0.12	-0.22	2.71	0.75	12.02	1.16
[BHB2007] 9	4350.	2.02	-0.37	-0.67	23.4	0.79	50.11	0.77
[BHB2007] 12	3009.	2.51	-1.12	-1.27	2.77	0.14	1.38	0.1
[BHB2007] 13NW	3514.	2.27	0.03	-0.03	0.088	0.23	≤ 1.0	0.68
[BHB2007] 14	4350.	2.02	0.05	-0.24	3.03	0.77	12.59	1.13
[BHB2007] 15	2841.	2.58	-0.90	-0.91	0.28	0.11	≤ 1.0	0.12
[BHB2007] 16	4590.	1.98	0.07	-0.09	2.77	0.88	13.18	1.24
[BHB2007] 18NE	3009.	2.51	-0.78	-0.94	1.28	0.14	≤ 1.0	0.13
[BHB2007] 18SW	3514.	2.27	-0.89	-1.04	6.71	0.34	13.2	0.46
[BHB2007] 19	3346.	2.37	-1.37	-1.47	16.6	0.26	19.1	0.27
[BHB2007] 20	3514.	2.27	-0.44	-0.60	1.37	0.30	3.47	0.50
V359 Oph	4060.	2.11	-0.36	-0.36	2.42	0.61	10.47	1.02
Lk H α 345	4060.	2.11	-0.19	-0.39	2.83	0.63	10.96	1.00
[CLR2010] 2NE	3346.	2.37	-0.59	-0.72	1.28	0.22	2.19	0.33
[CLR2010] 2SW	3009.	2.51	-0.70	-0.84	0.54	0.13	≤ 1.0	0.14

reliable spectroscopic and photometric information.

The stellar ages presented in Table 6 allow us to identify the characteristic timescale over which B59 has been actively forming stars. We calculate this timescale as the median age of all likely B59 members with reliable age estimates (i.e., all YSOs listed in Table 6 except [CLR2010] 2 NE & SW, which may not be linked to B59). We prefer the median to a standard mean because it is more robust to outliers with extreme ages (e.g., [BHB2007] 19). B59’s median stellar age, as inferred from DM98 PMS tracks using veiling-corrected luminosity estimates (L_{stel}), is 2.6 Myrs.

Our confidence in the age estimates we calculate here is reinforced by our ability to independently reproduce the age estimate derived by Luhman & Rieke (1999) for their sample of ρ Oph members. Following Luhman & Rieke (1999) by comparing each star’s total (non-veiling corrected) luminosity to the DM98 tracks, and adopting their estimated distance of 166 pc. ($m - M = 6.1$), we measure a median stellar age for ρ Oph of 0.21 Myrs, consistent with the ~ 0.3 Myr median stellar age Luhman & Rieke (1999) derived.

We also measured median stellar ages for other, well studied young clusters to provide an indication of B59’s relative, rather than absolute, age. These cluster age measurements require YSOs catalogs with measured spectral types and JHK photometry to estimate extinction and veiling corrected stellar luminosities using the same algorithms we applied to B59’s YSOs. Studies by Luhman and collaborators provide such catalogs for YSOs in Taurus, Rho Ophiuchus, and Chameleon (Luhman & Rieke 1999; Luhman et al. 2006; Luhman 2007). We have placed these objects on the HR diagram using the same routines applied to our B59 data, adopting the following distances to each region: Taurus – 140 pc., Oph – 126 pc., Cha – 170 pc (Kenyon et al. 2008; Wilking et al. 2008; Luhman 2008). Table 7 presents the median stellar age implied for each cluster by the DM98 and Baraffe et al. (1998) PMS tracks, and Figure 9 shows the locations of each region’s YSOs in the HR diagram.

Our analysis of the ages of YSOs in other regions,

however, lacks the iterative refinement of each YSO’s veiling estimate according to the agreement between the strengths of spectral features in the target and artificially veiled standard spectrum. Instead, for YSOs in other regions, we simply adopt the mean CTTS J band veiling measured by Cieza et al. (2005), which implicitly assumes that CTTSs dominate the population of each star forming region. This J band excess is an overestimate of the minimal veiling flux detected from WTTSs, however, such that we will under-estimate WTTSs intrinsic stellar luminosity, and thus overestimate their age. Our age estimates for Taurus, ρ Oph and Chameleon will therefore be slightly biased towards older ages in proportion to the number of WTTSs in the sample: we expect this to be a minimal effect for Taurus and ρ Oph, but potentially of some importance for the age we measure for the Chameleon star forming region.

3.6. Uncertainties in Derived Ages

Our measurement of B59’s median stellar age is subject to a few distinct statistical and systematic uncertainties. These affect the relative and absolute precision of our measurement in different ways, so we discuss them each below.

3.6.1. Random/Statistical Age Uncertainties

Our measurement of cluster median stellar ages are susceptible to (presumably) random uncertainties due to observational error and sampling effects. Age uncertainties introduced by observational errors are straightforward: errors in a YSO’s temperature and luminosity will shift its location in the HR diagram, corresponding to an error in the inferred mass and/or age. In the temperature/luminosity regime occupied by B59’s YSOs, luminosity is primarily sensitive to a star’s age, while its temperature is a better indicator of its mass. We therefore estimate the age errors that could be introduced by uncertainties in our luminosity estimates: we find that a 0.3 dex luminosity error corresponds to an age error of $\sim 125\%$. This is, however, the error in any individual age estimate: as we are determining the median stellar age of

TABLE 7
MEDIAN CLUSTER AGES

Cluster	N_{stars}	DM98 Median Age (Myrs)	B98 Median Age (Myrs)	Statistical Uncertainty (1σ)	Systematic Uncertainty
B59	18	2.59	4.37	29%	100–175%
Taurus	224	1.53	2.63	9%	100–175%
ρ Oph	61	1.04	3.63	16%	100–175%
Chameleon	185	2.59	3.02	9%	100–175%

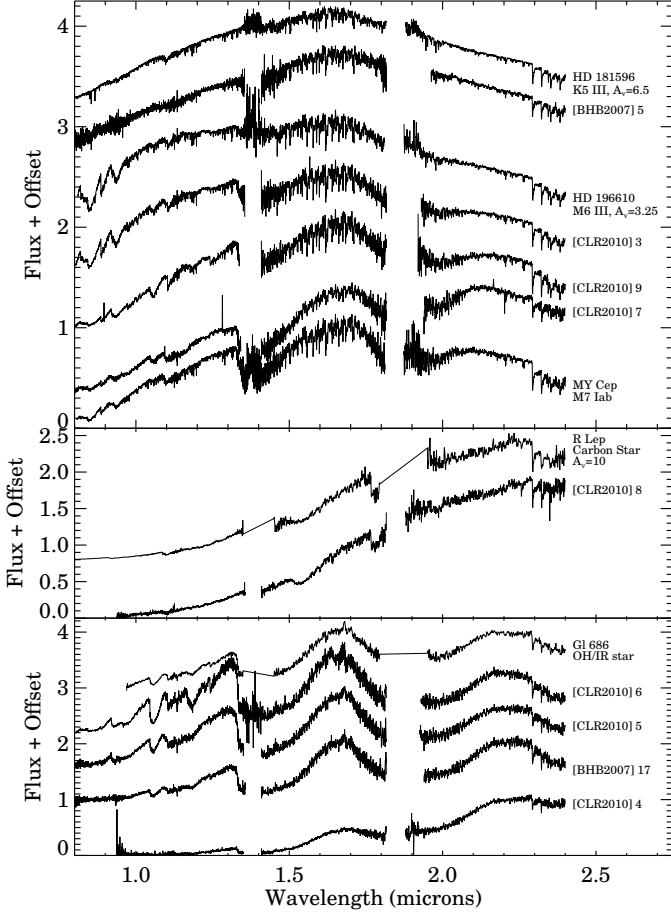


FIG. 5.— Spectroscopically identified giant stars in B59 and the Pipe Nebula. *Top*: K & M giants and supergiants – [BHB2007] 5, [CLR2010] 3, 7, & 9, shown in comparison to spectra of HD 181596 (K5 III), HD 156014 (M6 III), and MY Cep (M7 I) from the IRTF spectral library (Cushing et al. 2005). HD 181596 and HD 196610 have been artificially reddened to better match the target spectra. *Middle*: Carbon stars – [CLR2010] 8 shown for comparison with the reddened spectrum of R Lep (Lançon & Wood 2000). *Bottom*: OH/IR stars – [CLR2010] 4, 5 & 6, as well as [BHB2007] 17, shown for comparison with the spectrum of OH/IR star Gl 686, from Lançon & Wood (2000).

all the YSOs in each cluster, we can expect that this error will scale like $\sqrt{N_{cluster}}$. We calculate an estimate of the statistical uncertainty in each cluster’s median stellar age as $\frac{125\%}{\sqrt{N_{cluster}}}$, and present the resulting uncertainty in Table 7.

Sampling errors are perhaps the more subtle effect, but could be important for a sparse cluster like B59. A simple demonstration of this effect can be seen by examining the ages inferred for the 18 B59 YSOs listed in Table 6. The median age of these B59 YSOs, as inferred from the DM98 models, is bounded by the 2.42 Myr and 2.59 Myr ages estimated for V359 Oph and [BHB2007] 3, respectively the 9th and 10th oldest YSOs in the list. The relatively narrow age range bounding the median, however, is somewhat misleading. There are at least three B59 YSOs that were too heavily embedded to be observationally accessible to SpeX: [BHB2007] 10 and 11, classified as Class 0/I and Class I sources by Brooke et al. (2007), and 2M17112255, discovered and classified as a Class I system by Riaz et al. (2009). These YSOs are presumably quite young: arbitrarily assigning them ages of 0.5 Myrs would shift the age ordering such that the YSO defining B59’s median stellar age would be [BHB2007] 20, with an age of 1.37 Myrs according to the DM98 models. This would represent a $\sim 50\%$ age error, somewhat larger than the 30% age estimate predicted by the simple $\sqrt{N_{cluster}}$ calculation described above. We lack, however, a robust statistical description of the effect, so merely caution the reader that the formal statistical uncertainties reported in Table 7 may be underestimates for a sparse cluster like B59.

3.6.2. Systematic Age Uncertainties: Veiling Corrected Luminosities

One systematic effect which could affect our age estimates concerns the treatment of veiling flux in calculating each YSO’s luminosity. Deriving ages from each YSO’s total luminosity, rather than the veiling corrected stellar luminosity, typically reduces the YSO’s implied age by ~ 1.5 Myrs over the range of ages considered here. The median stellar age implied for B59 by comparing each YSO’s total, non-veiling corrected luminosity estimate to the DM98 tracks is 0.87 Myrs, as opposed to the veiling corrected age estimate of 2.6 Myrs. This represents a nearly 75% decrease in the cluster’s median stellar age, demonstrating that correctly accounting for veiling luminosity is necessary to accurately infer a YSO’s age. As the PMS tracks considered here do not account for emission from accretion or a circumstellar disks, we believe the correct approach is to infer ages from veiling-corrected luminosity estimates. We caution the reader, however, that many other investigators adopt non-veiling corrected bolometric luminosity estimates to derive YSO ages: as demonstrated above, this difference in approach results in age differences of 50–100%, and should be carefully considered in reconciling our results with other studies in the literature.

3.6.3. Systematic Age Uncertainties: Adopted PMS Tracks

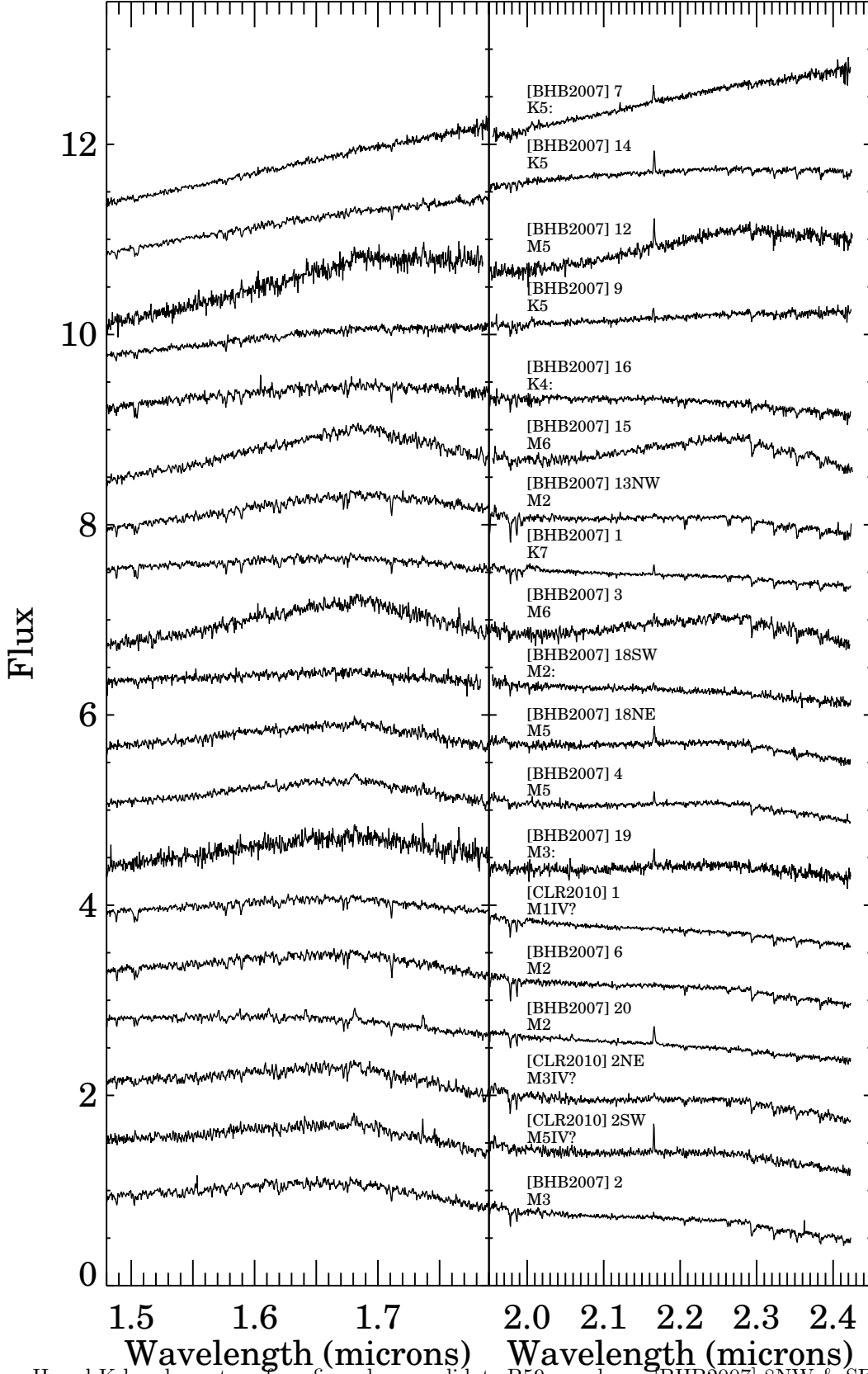


FIG. 6.— H and K band spectra of confirmed or candidate B59 members. [BHB2007] 8NW & SE are not shown, as their spectra are very low signal-to-noise.

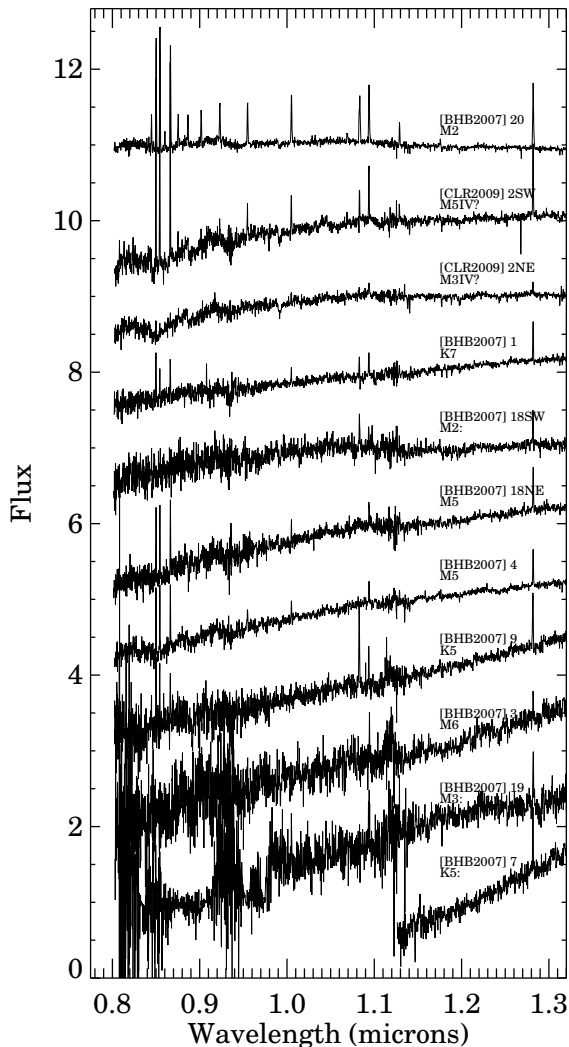


FIG. 7.— J band spectra of confirmed or candidate B59 members with visible J band emission lines.

As shown by Hillenbrand et al. (2008), the choice of PMS models from which to infer YSO ages has a significant affect on the absolute age derived for a given cluster. Hillenbrand et al. (2008) found that the PMS models computed by DM98 and Baraffe et al. (1998) predict the youngest and oldest ages, respectively, for a YSO of a given temperature and luminosity. We therefore use these two sets of model tracks to span the full range of B59’s potential absolute age. Using the same veiling corrected luminosities derived above for B59’s YSOs, but inferring ages from the $\alpha = 1$ PMS tracks calculated by Baraffe et al. (1998), results in a median stellar age for B59 of 4.4 Myrs, or roughly 70% older than the median stellar age inferred from the DM98 models.

Model dependent age differences are often attributed to luminosity offsets between equal age isochrones in two sets of PMS tracks. This suggests that, while the absolute ages predicted by two sets of PMS tracks may differ, they should produce similar *relative* age orderings for a given sample of clusters. Table 7 reveals, however, that this simple expectation is not necessarily borne out in

practice: both sets of models indicate that B59 has the oldest median stellar age, but the DM98 models imply that ρ Oph is *younger* than Taurus and Chameleon, while the Baraffe et al. (1998) models identify ρ Oph as *older* than Chameleon and Taurus.

These different relative age orderings arise from differences in the stellar population sampled in each cluster, combined with distinct isochrone slopes predicted by the two sets of PMS tracks. The temperature dependent offset between the 5 Myr DM98 and Baraffe isochrones is shown in the left panel of Figure 10. The Baraffe models imply consistently older ages for a given HR diagram location, but the age difference increases rapidly towards higher T_{eff} . This means that the relative age orderings of single stellar populations may not be preserved across models if the YSOs observed sample different temperature ranges. This is precisely the cause of the different relative ages inferred for ρ Oph in the DM98 and Baraffe models: as demonstrated in the right panel of Figure 10, the median temperature of the ρ Oph cluster stars is significantly larger than that of the other clusters analyzed here.

3.6.4. Systematic Age Uncertainties: Cluster Distances

Uncertainties in a cluster’s distance can also introduce errors in the inferred age: a closer distance implies a lower luminosity, and thus an older age, for a YSO of a given apparent magnitude. A concrete example of this effect is provided by ρ Oph, whose distance has recently been revised to ~ 125 parsecs from a previous estimate of ~ 160 parsecs. The 0.3 Myr estimate of ρ Oph’s age derived by Luhman & Rieke (1999) was based on the 160 parsec distance estimate. Replicating their analysis with a revised distance of 125 parsecs increases the derived median stellar age to 0.63 Myrs, twice as old as the previous estimate. Estimates of the distance to B59 and/or the Pipe Nebula are scarce: the two most recent distances measured for the Pipe are 130^{+13}_{-20} parsecs and 145 ± 16 parsecs, obtained by Lombardi et al. (2006) and Alves & Franco (2007), respectively. We have adopted the Lombardi et al. (2006) distance for the luminosity and age measurements presented here, but we note that the Alves & Franco (2007) distance implies in a median stellar age (inferred from veiling corrected luminosities and DM98 tracks) for B59 of 1.7 Myrs, or decreased by roughly 35% from our primary age estimate.

3.6.5. Total Error Budget for B59’s Age Estimate

In summary, our measurement of B59’s absolute age is subject to statistical errors at the $\sim 30\%$ level, such that B59’s median stellar age (adopting veiling corrected luminosities and inferred from the DM98 models) is 2.6 ± 0.8 Myrs. Several systematic uncertainties could shift the median stellar age derived for B59, however, by as much as 100%. Adding these effects in quadrature, we find that systematic uncertainties could introduce errors as large as 150% into our measurement of B59’s absolute age. Including potential systematic effects therefore revises the error budget for B59’s median (DM98) stellar age to $2.6^{+4.1}_{-2.6}$ Myrs.

4. DISCUSSION

4.1. The Star Formation Timescale in B59

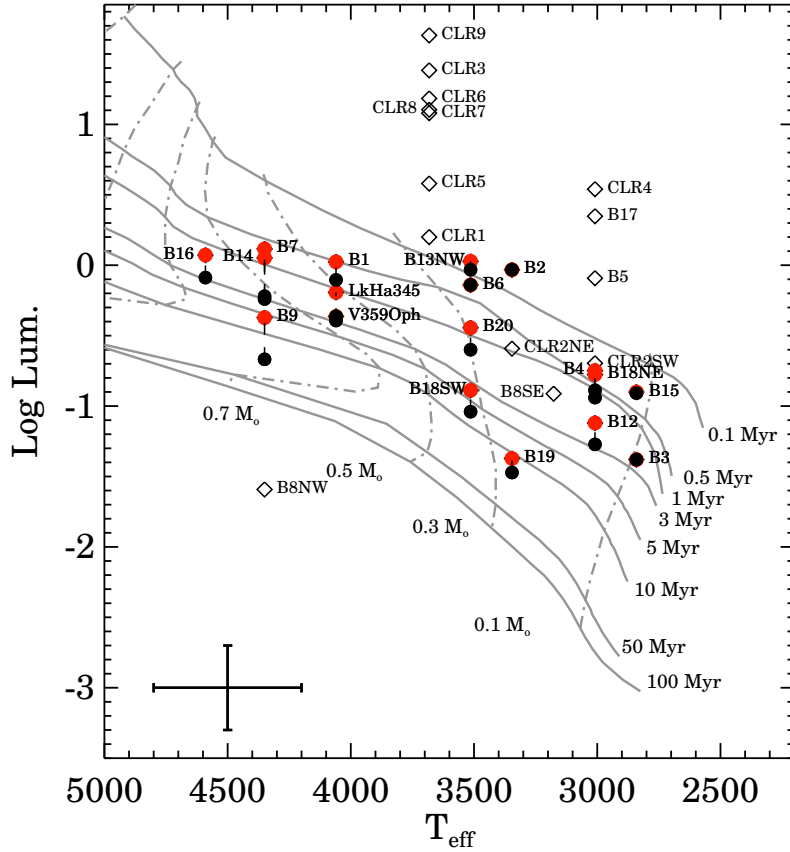


FIG. 8.— B59 HR diagram calculated using JHK photometry. Likely B59 members (including previously studied members V359 Oph & Lk H α 345) are shown twice; red dots indicate their total bolometric luminosity, and black dots indicate their stellar luminosity after subtracting H band veiling. Objects classified as background giants are shown with open diamonds, as are [BHB2009] 8SE & NW, whose spectra are too noisy for reliable HR diagram placement. The DM98 model grid is shown for comparison as solid and dotted lines.

The prompt star formation paradigm agrees well with the evolutionary timescales expected for dense cores that lack significant internal or external support. Acted on by gravity alone, a core should collapse in roughly one free-fall time, $\tau_{ff} = (3\pi/32G\rho)^{1/2}$. Hydrodynamic models of undriven turbulent molecular clouds predict only slightly longer evolutionary timescales, as the turbulent support dissipates on ~ 1 -2 free-fall timescales (Klessen et al. 2000). Offner et al. (2008), for example, find that star formation activity ceases after $0.75 \tau_{ff}$ in their simulations of star formation within undriven turbulent molecular cores.

The uncertainties associated with our measurement of B59's age are sizable, but the most straightforward interpretation of this result is that star formation activity began in B59 nearly 3 Myrs ago. The presence of heavily embedded (and presumably young) Class 0/I objects within B59 (Brooke et al. 2007; Riaz et al. 2009) also implies that this star formation activity has persisted to the present day. If the oldest stars in B59 formed from the dense core currently associated with the cluster, these observations would indicate a lower limit of 3 Myrs for the core's lifetime. A star formation timescale for B59 comparable to 3 Myrs is by no means startling in ab-

solute terms. Indeed, while the stellar content of B59 appears somewhat older than that of the ρ Oph, Taurus, and Chameleon star forming regions, the inferred star formation timescales agree to within a factor of two.

Expressing B59's age in units of the core free-fall time and the core's crossing time is also useful for interpreting the core's physical evolution. Adopting the density ($n(\text{H}_2) = 10^4 \text{ cm}^{-3}$; $\rho = 3.5 \times 10^{-20} \text{ g cm}^{-3}$), radius ($R = 0.19 \text{ parsecs} = 5.9 \times 10^{12} \text{ km}$), and velocity dispersion ($\sigma_v = 0.37 \text{ km/sec}$, calculated from 0.86 km/sec FWHM) tabulated for the B59 dense core by Rathborne et al. (2009), we calculate $\tau_{ff} \sim 0.35 \text{ Myrs}$ and $\tau_{cross} \sim 0.5 \text{ Myrs}$. These calculations describe B59's current state; if B59 is evolving from a lower density to higher density configuration, these timescales would have been somewhat longer in the past than they are today. Intensive observations of the dense gas within B59 have not revealed any kinematic signatures of rapid collapse (Rathborne et al. 2009). If B59 is evolving relatively quiescently, the timescales we derive today are likely comparable to those of B59's recent past.

The uncertainties on B59's age permit that star formation may have begun as recently as the core's last dynamical time, or as long as ~ 13 dynamical timescales ago.

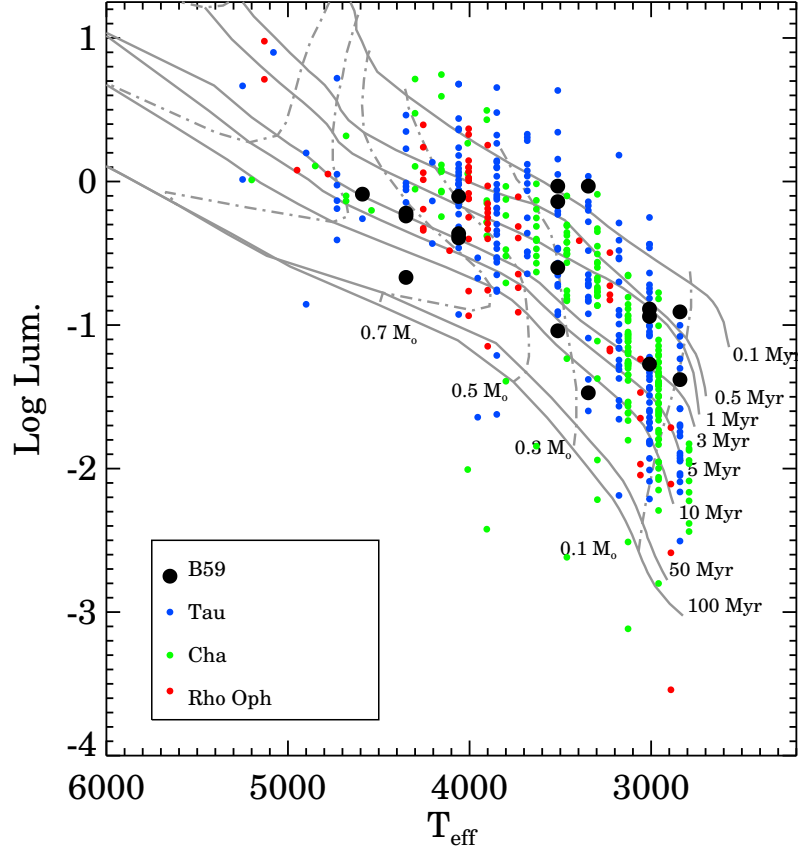


FIG. 9.— HR diagram locations for YSOs in nearby young clusters, calculated using JHK photometry and assuming stellar luminosities (subtracting off H band veiling). B59 sources are shown as black dots, Rho Ophiuchus sources are shown in red, Taurus sources are shown in blue, and Chameleon sources are shown in green. The DM98 model grid is shown for comparison with solid and dotted lines corresponding to isochrones and fixed mass evolutionary tracks, respectively.

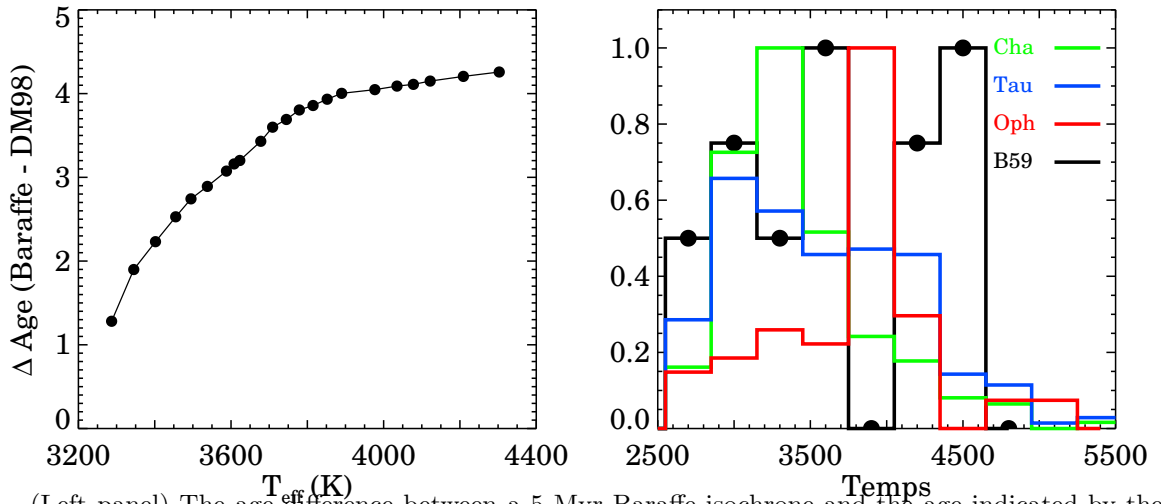


FIG. 10.— (Left panel) The age difference between a 5 Myr Baraffe isochrone and the age indicated by the DM98 models for the same location in the HR diagram, presented as a function of T_{eff} . (right panel) T_{eff} s of the stars sampled from each cluster analyzed here. The Cha & Taurus samples are dominated by cooler stars, where the disparity between the B98 and DM98 models is ~ 1 Myr. B59 and ρ Oph are successively warmer: at these temperatures, the DM98 and B98 models predict ages that can differ by 4 Myrs.

The maximum likelihood value, however, suggests that B59 has been forming stars for ≈ 6 crossing or free fall times. Extinction maps of B59 also indicate that the core is spatially coherent, having not undergone significant fragmentation as it formed stars (Román-Zúñiga et al. 2009). Taken at face value, the maximum likelihood value of B59’s star formation timescale suggests that B59 could join a short, but growing, list of dense cores that appear to have resisted global collapse and sustained ongoing star formation for several dynamical times. Swift & Welch (2008) examined the dense gas and stellar population of the L1551 star forming region, demonstrating that L1551 has been forming stars for ~ 5 Myrs, or $\geq 5 \tau_{ff}$; they identify stellar feedback as a likely source of support against collapse within this region. As we find for B59, Swift & Welch (2008) also find that L1551 contains stars over a broad range of evolutionary stages (Class 0 through III). Similar results have been reported for the young cluster AGFL961; Williams et al. (2009) conclude that either disk evolution proceeds more rapidly in clustered environments, or that star formation persists in clusters over several dynamical timescales. Finally, Tan et al. (2006) present observationally-based calculations that suggest ages of $\sim 3\text{--}4 \tau_{ff}$ for several rich young clusters that are still forming stars (ie, ρ Oph, IC 348, ONC, etc.). These measurements suggest that some dense cores can sustain star formation over a few dynamical timescales, including in relatively low-mass cores like B59, which does not appear to host massive stars.

What physical mechanism could be supporting these cores against collapse, extending their lifetimes beyond that expected for cores in free fall collapse? As noted above, one possibility is stellar outflows: Matzner (2007) calculate that outflows may support clusters against collapse for several crossing times. This mechanism could explain B59’s relative stability, particularly given that Onishi et al. (1999) and Riaz et al. (2009) find evidence for an active outflow within the B59 core. A recent ammonia survey of the Pipe, however, finds little evidence for significant non-thermal motions within B59’s dense gas, as would be expected if bulk outflow motions are the core’s main support against gravitational collapse (Román-Zúñiga et al. 2009; Rathborne et al. 2008). High-resolution observations of the kinematics of B59’s dense gas are required to clarify the extent to which it (and, by extension, outflows from previous generations of protostars) could support B59 against collapse.

The collapse of a molecular core may also be strongly affected by radiative feedback from the young protostars it contains. Krumholz, Klein & McKee (2007) used simulations of massive molecular cores to demonstrate that protostars can contribute significant heating to a collapsing core, thereby suppressing fragmentation. This heating does not, however, appear to slow mass accretion and collapse within the core: much of the radiation ‘leaks’ out of optically thin holes in the core (Krumholz et al. 2009). Offner et al. (2009) extended this investigation into the regime of low-mass star formation, finding a similar reduction in stellar multiplicity due to reduced fragmentation, as well as a significant reduction in the mass accretion rate of the earliest formed protostar. These simulations suggest that radiative feedback could play some role in extending B59’s star formation timescale.

Magnetic fields are a final physical mechanism that

is often invoked to support cloud cores against collapse. Magnetic fields have been a fundamental component of star formation models for decades (Nakano 1984; Shu et al. 1987; Mouschovias & Ciolek 1999), but observational constraints on the strengths of magnetic fields within molecular clouds are difficult to obtain (e.g., Crutcher et al. 2009). Past measurements suggest magnetic fields may contribute appreciable amounts of support to molecular cores (Troland & Crutcher 2008), and recent polarization measurements in the Pipe Nebula indicate the presence of a $\sim 17 \mu\text{G}$ magnetic field within B59 itself (Alves et al. 2008). This suggests that magnetic fields may be providing B59 with some support against collapse, but this is a relatively weak statement: magnetic fields can extend a dense core’s lifetime arbitrarily, depending on the field strength adopted.

4.2. The Star Formation Efficiency of B59

As the discussion above demonstrates, there are several mechanisms which could plausibly explain B59’s maximum likelihood star formation timescale. To provide additional leverage for comparing observations of B59 with predictions of theoretical models of star forming cores, we now consider B59’s star formation efficiency in addition to its characteristic timescale.

B59’s present-day star formation efficiency (SFE) can be characterized as the mass of the cluster’s stellar population divided by the core’s initial gas mass. The total mass of all B59 YSOs analyzed here is $\sim 8 M_\odot$ according to the DM98 models, and $12 M_\odot$ according to the Baraffe et al. (1998) models. Brooke et al. (2007) and Riaz et al. (2009) also provide preliminary mass estimates for [BHB2007] 10, 11, and 2M12112255, the B59 YSOs that were too heavily embedded to be observed with SpEx. These embedded YSOs contribute an additional $0.7 M_\odot$ to B59’s total stellar mass, bringing B59’s total stellar mass to $\sim 9\text{--}13 M_\odot$.

B59’s initial gas mass can be approximated as the sum of its stellar and gas masses. Extinction maps indicate that B59 contains $\sim 20 M_\odot$ of dense gas, implying an initial core mass of $\sim 29\text{--}33 M_\odot$. This suggests B59’s present-day SFE is $\sim 30\text{--}40\%$, depending on the choice of models used to infer stellar masses. Combining this SFE with B59’s median stellar age produces an estimate of the SFE/τ_{ff} of the B59 dense core. B59’s sizable age uncertainty translates into a large range of allowed SFE/τ_{ff} values: $3\text{--}40\%$, though the probability distribution is strongly asymmetric, peaking at a maximum likelihood value of $\sim 6\%$.

The SFE/τ_{ff} values predicted by theoretical models for star forming cores cover a large range, with slower star formation rates corresponding to models incorporating some additional physical mechanism (driven turbulence, magnetic fields, outflows, etc.) to support cores against collapse. Unsupported models typically produce SFE/τ_{ff} values $\sim 10\text{--}20\%$, while models that incorporate additional support often predict proportionally lower SFE/τ_{ff} values. As one example, the moderately supercritical (ie, prone to gravitational collapse) magnetic models of Vázquez-Semadeni et al. (2005) produced SFE/τ_{ff} values $\sim 5\%$, whereas earlier non-magnetic models by the same authors produced SFE/τ_{ff} values $\sim 15\%$ (Vázquez-Semadeni et al. 2003). The magnetically subcritical models of Nakamura & Li

(2008), which also incorporate feedback from stellar outflows, produce SFE/τ_{ff} values of 1% or less.

The theoretical models calculated by Price & Bate (2009) are arguably the best match to B59’s actual physical structure. These models (indicated hereafter as ‘the PB09 model grid’) incorporate both magnetic fields and radiative feedback, and follow the evolution of a cloud core whose mass ($50 M_{\odot}$) and radius (~ 0.2 pc) are reasonably close to the values which likely characterized B59 prior to the onset of active star formation. The PB09 model grid spans magnetic fields of various strengths, but all models were supercritical, with mass-to-flux ratios ranging from 3 to ∞ . Though the models were only allowed to evolve over a timespan corresponding to $1.5 \tau_{ff}$, or $0.35\text{--}0.5 \tau_{ff}$ following the formation of the first star in the core, the implied SFE/τ_{ff} values range from $\sim 30\%$ for the model lacking both magnetic fields and radiative feedback, to $\sim 6\%$ for the model incorporating radiative feedback and the strongest magnetic field ($B_0 = 65 \mu\text{G}$). In analyzing the range of star formation efficiencies produced by their model grid, PB09 note that magnetic fields appear to play a more important role than radiative feedback in quenching star formation.

B59’s maximum likelihood SFE/τ_{ff} value of $\sim 6\%$ is contained within the range of values predicted by the PB09 models, but B59’s observed magnetic field strength ($B \sim 17 \mu\text{G}$) is only $\sim 1/4$ that adopted in the least efficient PB09 model ($B \sim 65 \mu\text{G}$). The PB09 models and the present-day B59, however, represent significantly different time periods in the evolution of a star forming core. It would be interesting to see what properties the PB09 models might have if they were allowed to evolve to $\sim 5 \tau_{ff}$: would the magnetic field diffuse out of the core, such that the measured magnetic field strength would better agree with what we observe in B59 today?

It is too early to draw detailed conclusions, but the agreement between B59’s observed properties and the predictions of the PB09 model grid are intriguing, and suggest that magnetic support and radiative feedback help support B59 against collapse.

4.3. The Spatial Extent of Star Formation in Pipe

The suggestion that magnetic fields may be important for understanding star formation within the Pipe Nebula is also consistent with the results of the polarization survey conducted by Alves et al. (2008). Alves et al. (2008) measure a significant spatial gradient in the component of the Pipe’s magnetic field aligned with the plane of the sky, ranging from $\sim 17 \mu\text{G}$ in B59 to $\sim 65 \mu\text{G}$ in the Pipe’s ‘Bowl’. As Alves et al. (2008) indicate, this gradient correlates with star formation activity: the weakest, most poorly aligned field vectors lie in B59, where the bulk of the Pipe’s star formation activity is taking place, while areas with stronger, better aligned magnetic field vectors appear devoid of star formation activity.

In this context, it is interesting to note the location of [CLR2010] 2, the candidate YSO identified by Forbrich et al. (2009) in their MIPS survey of the Pipe, and subsequently confirmed as a likely YSO by our spectroscopic analysis. This candidate YSO lies in the Pipe’s ‘Stem’, where the magnetic field appears to be stronger than in B59, but not as strong as in the Bowl. This YSO also displays a rich emission line spectrum, suggesting it is a young, heavily accreting YSO, which would be con-

sistent with a picture in which star formation activity was just beginning in the Neck of the Pipe. We note, however, that [CLR2010] 2 does not appear to be heavily embedded; indeed, [BHB2007] 10 and 11 appear to be in significantly earlier evolutionary stages than [CLR2010] 2, making it difficult to conclude that the onset of star formation activity is simply progressing linearly from B59 towards the Bowl of the Pipe.

5. SUMMARY

1. We obtained and analyzed JHK SpeX spectra for 20 candidate B59 YSOs, and 10 additional mid-IR bright sources throughout the larger Pipe Nebula. We measured temperature and luminosity sensitive spectral indices from these spectra, and determined the extinction, NIR color excesses, and spectral type required to self-consistently reproduce each target’s spectral energy distribution. This analysis leads us to re-classify [BHB2007] 5 and 17, previously identified as candidate B59 members, as background giants, and to identify [CLR2010] 2 SW as a promising candidate YSO in the stem of the Pipe. None of the mid-IR bright candidates outside of the Stem of the Pipe were found to be YSOs
2. For each candidate B59 YSO with reliable spectra and photometry, we derived effective temperatures and luminosities, with and without correction for non-photospheric flux. Using these measurements to place each YSO in the HR diagram, we inferred ages and masses for each YSO from theoretical pre-main sequence evolutionary tracks. B59’s median stellar age, as inferred from the DM98 models and accounting only for statistical uncertainties, is 2.6 ± 0.8 Myrs. Including potential systematic effects revises the error budget for B59’s median (DM98) stellar age to $2.6^{+4.1}_{-2.6}$ Myrs.
3. Comparing the median stellar ages implied for several star forming regions by different pre-main sequence evolutionary tracks demonstrates that the construction of even a relative age ordering requires careful attention to sampling of each region’s stellar population. Despite this sensitivity, both sets of tracks studied here imply that B59 is at least as old as, if not slightly older than, the more well-studied ρ Oph, Taurus, and Chameleon star forming regions. The dominant source of error in this conclusion is the uncertainty in the distance adopted to each cluster: we minimize other potential systematic errors by applying a consistent set of algorithms to a homogeneous set of catalogs of young stars in each cluster.
4. The maximum likelihood median stellar age we measure for B59, and the observed properties of the dense gas in the region, suggests that the B59 dense core may have been stable against collapse and actively forming stars for roughly 6 dynamical timescales, with a star formation efficiency per dynamical time of $\sim 6\%$, though the uncertainty in our age measurement permits a significant range of possible SFE/τ_{ff} values ($3\text{--}40\%$). These proper-

ties agree well with recent star formation simulations that incorporate sub-critical magnetic fields and radiative feedback from protostellar heating.

The authors owe a debt of gratitude to Bill Golisch, Paul Sears, and Bobby Bus for their generous assistance in obtaining efficient and accurate observations. KRC gratefully acknowledges Kevin Luhman’s assistance in providing homogeneous catalogs of spectral types and photometry for young stars in well known star forming regions, and helpful discussions with Lynne Hillenbrand and Michael Meyer concerning the practice and reliability of pre-main sequence age measurements, with Eric Mamajek on the history of star formation in the Sco-Cen region, and Stella Offner on the physics of collapsing cores. The authors also wish to recognize and acknowledge the very significant cultural role and reverence that the summit of Mauna Kea has always had within the indigenous Hawaiian community. We are most fortunate to have the opportunity to conduct observations from this mountain. NASA support was provided to K. Covey for this work through the Spitzer Space Telescope Fellowship

Program, through a contract issued by the Jet Propulsion Laboratory, California Institute of Technology under a contract with NASA.

This research has made use of NASA’s Astrophysics Data System Bibliographic Services, the SIMBAD database, operated at CDS, Strasbourg, France, the NASA/IPAC Extragalactic Database, operated by the Jet Propulsion Laboratory, California Institute of Technology, under contract with the National Aeronautics and Space Administration, and the VizieR database of astronomical catalogs (Ochsenbein et al. 2000). IRAF (Image Reduction and Analysis Facility) is distributed by the National Optical Astronomy Observatories, which are operated by the Association of Universities for Research in Astronomy, Inc., under cooperative agreement with the National Science Foundation.

The Two Micron All Sky Survey was a joint project of the University of Massachusetts and the Infrared Processing and Analysis Center (California Institute of Technology). The University of Massachusetts was responsible for the overall management of the project, the observing facilities and the data acquisition. The Infrared Processing and Analysis Center was responsible for data processing, data distribution and data archiving.

APPENDIX

TWA SPECTRAL STANDARDS

To supplement the spectral atlas presented by Cushing et al. (2005) with additional pre-main sequence spectral standards, we obtained SpeX SXD spectra of several members of the TW Hya moving group. Observed during the same nights as our B59 candidates, these spectra share the same instrumental set-up and reduction process as our target spectra. The H and K band portion of these spectra are shown in Figure 11, ordered such that earlier type objects are found higher in the figure. Spectral features sampled by the indices presented in §3.2 are also labeled.

As most B59 members are heavily reddened, the z and J band portion of their observed spectrum was typically quite noisy, and thus not useful for measuring spectral types. This region contains most of the H I Paschen series, the Ca II triplet and the He I 10830 Å line, however, which are often seen in emission in young, actively accreting stars. The 0.8-1.3 μm SpeX spectrum of TW Hya, an actively accreting CTTS, is shown in Figure 12 for comparison with Figure 7, which shows 0.8-1.3 μm spectra of candidate or confirmed B59 members with J band emission features.

To provide the community with moderate resolution NIR pre-main sequence spectral standards, we have made these spectra publicly available at <http://www.astro.cornell.edu/~kcovey/CoveyB59SpeX.tar.gz>.

REFERENCES

- Ali, B., Carr, J. S., Depoy, D. L., Frogel, J. A., & Sellgren, K. 1995, *AJ*, 110, 2415
- Allers, K. N. et al. 2007, *ApJ*, 657, 511
- Allers, K. N., et al. 2009, *ApJ*, 697, 824
- Alves, F. O., & Franco, G. A. P. 2007, *A&A*, 470, 597
- Alves, F. O., Franco, G. A. P., & Girart, J. M. 2008, *A&A*, 486, L13
- Alves, J., Lombardi, M., & Lada, C. J. 2007, *A&A*, 462, L17
- Aspin, C. 2003, *AJ*, 125, 1480
- Ballesteros-Paredes, J., & Hartmann, L. 2007, *Revista Mexicana de Astronomia y Astrofisica*, 43, 123
- Baraffe, I., Chabrier, G., Allard, F., & Hauschildt, P. H. 1998, *A&A*, 337, 403
- Barnard, E. E., Frost, E. B., & Calvert, M. R. 1927, A photographic atlas of selected regions of the Milky way, ed. E. E. Barnard, E. B. Frost, & M. R. Calvert
- Bastian, N., Covey, K. R., & Meyer, M. R. 2010, *ArXiv e-prints*
- Brooke, T. Y. et al. 2007, *ApJ*, 655, 364
- Carpenter, J. M. 2001, *AJ*, 121, 2851
- Cieza, L. A., Kessler-Silacci, J. E., Jaffe, D. T., Harvey, P. M., & II, N. J. E. 2005
- Covey, K. R. et al. 2008, *AJ*, 136, 1778
- . 2007, *AJ*, 134, 2398
- Crutcher, R. M., Hakobian, N., & Troland, T. H. 2009, *ApJ*, 692, 844
- Cushing, M. C., Rayner, J. T., & Vacca, W. D. 2005, *ApJ*, 623, 1115
- Cushing, M. C., Vacca, W. D., & Rayner, J. T. 2004, *PASP*, 116, 362
- D’Antona, F., & Mazzitelli, I. 1994, *ApJS*, 90, 467
- Doppmann, G. W., Greene, T. P., Covey, K. R., & Lada, C. J. 2005, *AJ*, 130, 1145
- Elmegreen, B. G. 2000, *ApJ*, 530, 277
- Forbrich, J., Lada, C. J., Muench, A. A., Alves, J., & Lombardi, M. 2009, *ApJ*, 704, 292
- Forbrich, J., Posselt, B., Covey, K. R., & Lada, C. J. 2010, *arXiv:1006.3556*
- Geballe, T. R., et al. 2002, *ApJ*, 564, 466
- Gorlova, N. I., Meyer, M. R., Rieke, G. H., & Liebert, J. 2003, *ApJ*, 593, 1074
- Hartmann, L., Ballesteros-Paredes, J., & Bergin, E. A. 2001, *ApJ*, 562, 852
- Herbig, G. H. 2005, *AJ*, 130, 815
- Hillenbrand, L. A. 1997, *AJ*, 113, 1733
- Hillenbrand, L. A., Bauermeister, A., & White, R. J. 2008, in *Astronomical Society of the Pacific Conference Series*, Vol. 384, 14th Cambridge Workshop on Cool Stars, Stellar Systems, and the Sun, ed. G. van Belle, 200–+
- Indebetouw, R., Whitney, B. A., Johnson, K. E., & Wood, K. 2005

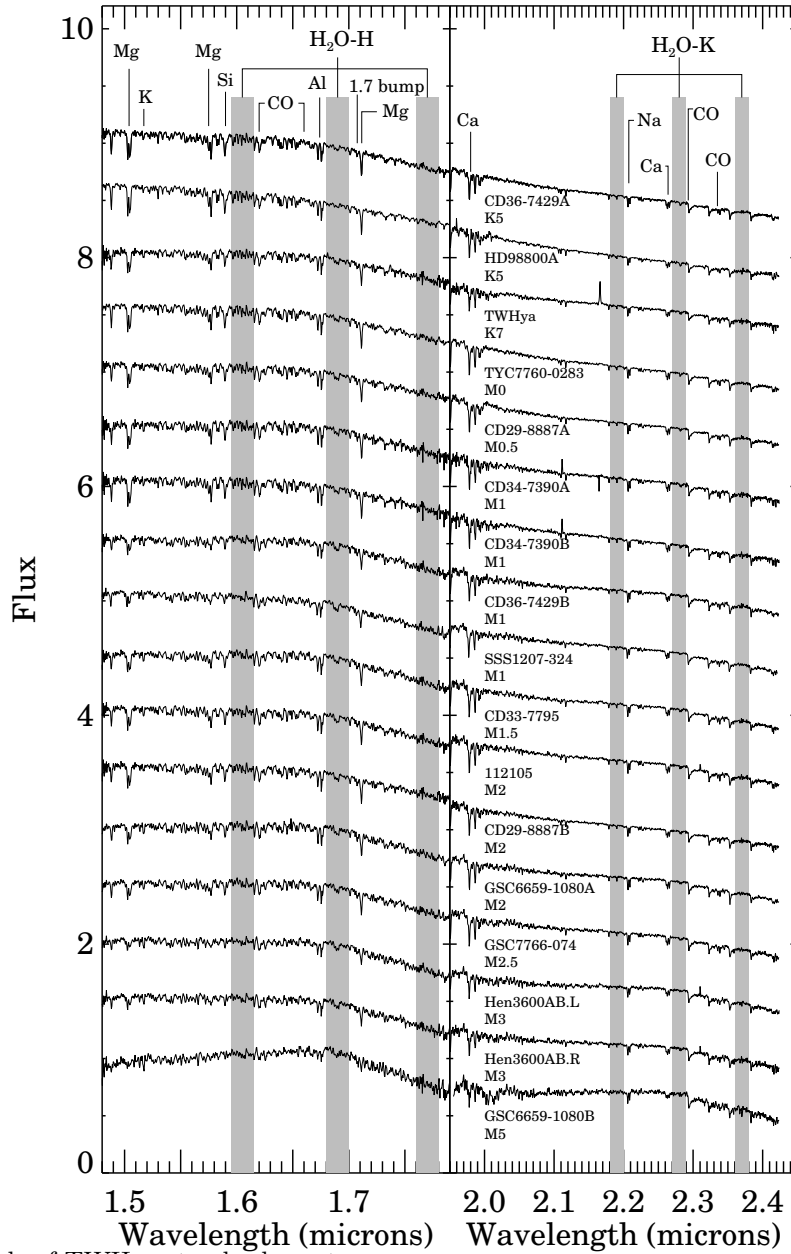


FIG. 11.— HK bands of TWHya standard spectra.

- Ivanov, V. D., Rieke, M. J., Engelbracht, C. W., Alonso-Herrero, A., Rieke, G. H., & Luhman, K. L. 2004, *ApJS*, 151, 387
- Kainulainen, J., Lada, C. J., Rathborne, J. M., & Alves, J. F. 2009, *A&A*, 497, 399
- Kenyon, S. J., Gómez, M., & Whitney, B. A. 2008, *Low Mass Star Formation in the Taurus-Auriga Clouds*, ed. B. Reipurth, 405–+
- Kenyon, S. J., & Hartmann, L. 1995, *ApJS*, 101, 117
- Kirkpatrick, J. D., Henry, T. J., & McCarthy, Jr., D. W. 1991, *ApJS*, 77, 417
- Kleinmann, S. G., & Hall, D. N. B. 1986, *ApJS*, 62, 501
- Klessen, R. S., Heitsch, F., & Mac Low, M.-M. 2000, *ApJ*, 535, 887
- Khoutek, L., & Wehmeyer, R. 2003, *Astronomische Nachrichten*, 324, 437
- Lada, C. J., Lombardi, M., & Alves, J. F. 2009
- Lada, C. J., Muench, A. A., Rathborne, J., Alves, J. F., & Lombardi, M. 2008, *ApJ*, 672, 410
- Lançon, A., & Wood, P. R. 2000, *A&AS*, 146, 217
- Lombardi, M., & Alves, J. 2001, *A&A*, 377, 1023
- Lombardi, M., Alves, J., & Lada, C. J. 2006, *A&A*, 454, 781
- Luhman, K. L. 2004, *ApJ*, 617, 1216
- . 2007, *ApJS*, 173, 104
- . 2008, *ArXiv e-prints*, 808
- Luhman, K. L., & Rieke, G. H. 1999, *ApJ*, 525, 440
- Luhman, K. L., Rieke, G. H., Lada, C. J., & Lada, E. A. 1998, *ApJ*, 508, 347
- Luhman, K. L., Whitney, B. A., Meade, M. R., Babler, B. L., Indebetouw, R., Bracker, S., & Churchwell, E. B. 2006, *ApJ*, 647, 1180
- Mac Low, M.-M., & Klessen, R. S. 2004, *Reviews of Modern Physics*, 76, 125
- Matzner, C. D. 2007, *ApJ*, 659, 1394
- McLean, I. S., McGovern, M. R., Burgasser, A. J., Kirkpatrick, J. D., Prato, L., & Kim, S. S. 2003, *ApJ*, 596, 561
- Merrill, P. W., & Burwell, C. G. 1950, *ApJ*, 112, 72
- Meyer, M. R., Calvet, N., & Hillenbrand, L. A. 1997, *AJ*, 114, 288
- Meyer, M. R., Edwards, S., Hinkle, K. H., & Strom, S. E. 1998, *ApJ*, 508, 397
- Morales-Calderón, M. et al. 2009, *ApJ*, 702, 1507

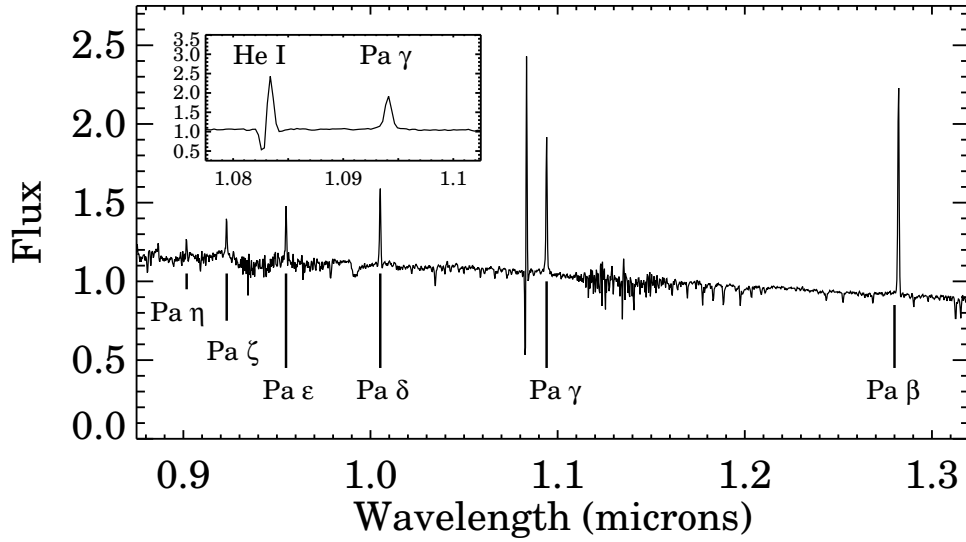


FIG. 12.— J band spectrum of TW Hydra to show rich emission line spectrum.

- Mouschovias, T. C., & Ciolek, G. E. 1999, in NATO ASIC Proc. 540: The Origin of Stars and Planetary Systems, ed. C. J. Lada & N. D. Kylafis, 305–+
- Muench, A. A., Lada, C. J., Rathborne, J. M., Alves, J. F., & Lombardi, M. 2007, *ApJ*, 671, 1820
- Muench, A. A., Lada, E. A., Lada, C. J., & Alves, J. 2002, *ApJ*, 573, 366
- Mentuch, E., Brandeker, A., van Kerkwijk, M. H., Jayawardhana, R., & Hauschildt, P. H. 2008, *ApJ*, 689, 1127
- Nakamura, F., & Li, Z.-Y. 2008, *ApJ*, 687, 354
- Nakano, T. 1984, *Fundamentals of Cosmic Physics*, 9, 139
- Ochsenbein, F., Bauer, P., & Marcout, J. 2000, *A&AS*, 143, 23
- Offner, S. S. R., Klein, R. I., & McKee, C. F. 2008, *ApJ*, 686, 1174
- Ojha, D. K., Tej, A., Schultheis, M., Omont, A., & Schuller, F. 2007, *MNRAS*, 381, 1219
- Onishi, T. et al. 1999, *PASJ*, 51, 871
- Price, D. J., & Bate, M. R. 2009, *ArXiv e-prints*
- Rathborne, J. M., Lada, C. J., Muench, A. A., Alves, J. F., Kainulainen, J., & Lombardi, M. 2009, *ApJ*, 699, 742
- Rathborne, J. M., Lada, C. J., Muench, A. A., Alves, J. F., & Lombardi, M. 2008, *ApJS*, 174, 396
- Rayner, J. T., Toomey, D. W., Onaka, P. M., Denault, A. J., Stahlberger, W. E., Vacca, W. D., Cushing, M. C., & Wang, S. 2003, *PASP*, 115, 362
- Reid, I. N., Burgasser, A. J., Cruz, K. L., Kirkpatrick, J. D., & Gizis, J. E. 2001, *AJ*, 121, 1710
- Reipurth, B., Nyman, L.-A., & Chini, R. 1996, *A&A*, 314, 258
- Riaz, B., Martín, E. L., Bouy, H., & Tata, R. 2009, *ApJ*, 700, 1541
- Román-Zúñiga, C. G., Lada, C. J., & Alves, J. F. 2009, *ApJ*, 704, 183
- Román-Zúñiga, C. G., Lada, C. J., Muench, A., & Alves, J. F. 2007, *ApJ*, 664, 357
- Sestito, P., Palla, F., & Randich, S. 2008, *A&A*, 487, 965
- Shu, F. H., Adams, F. C., & Lizano, S. 1987, *ARA&A*, 25, 23
- Slesnick, C. L., Hillenbrand, L. A., & Carpenter, J. M. 2004, *ApJ*, 610, 1045
- Smith, R. J., Clark, P. C., & Bonnell, I. A. 2008, *MNRAS*, 391, 1091
- . 2009, *ArXiv e-prints*
- Stephenson, C. B., & Sanduleak, N. 1977, *ApJS*, 33, 459
- Swift, J. J., & Welch, W. J. 2008, *ApJS*, 174, 202
- Swift, J. J., & Williams, J. P. 2008, *ApJ*, 679, 552
- Takagi, Y., Itoh, Y., & Oasa, Y. 2010, *PASJ*, 62, 501
- Tan, J. C., Krumholz, M. R., & McKee, C. F. 2006, *ApJ*, 641, L121
- The, P.-S. 1964, *Contributions from the Bosscha Observatory*, 27, 1
- Troland, T. H., & Crutcher, R. M. 2008, *ApJ*, 680, 457
- Vacca, W. D., Cushing, M. C., & Rayner, J. T. 2003, *PASP*, 115, 389
- Vázquez-Semadeni, E., Ballesteros-Paredes, J., & Klessen, R. S. 2003, *ApJ*, 585, L131
- Vázquez-Semadeni, E., Kim, J., & Ballesteros-Paredes, J. 2005, *ApJ*, 630, L49
- Wallace, L., & Hinkle, K. 1997, *ApJS*, 111, 445
- Wilking, B. A., Greene, T. P., & Meyer, M. R. 1999, *AJ*, 117, 469
- Weights, D. J., Lucas, P. W., Roche, P. F., Pinfield, D. J., & Riddick, F. 2009, *MNRAS*, 392, 817
- Wilking, B. A., Gagné, M., & Allen, L. E. 2008, *Star Formation in the ρ Ophiuchi Molecular Cloud*, ed. B. Reipurth, 351–+
- Williams, J. P. et al. 2009, *ApJ*, 699, 1300